

Tracking the Progression of Anion Reorientational Behavior between α -phase and β -phase Alkali-Metal Silanides MSiH_3 by Quasielastic Neutron Scattering

Mirjana Dimitrievska,^{†,‡,*} Jean-Noël Chotard,[§] Raphaël Janot,[§] Antonio Faraone,[†] Wan Si Tang,^{†,‡,Δ} Alexander V. Skripov,[#] and Terrence J. Udovic[†]

[†]NIST Center for Neutron Research, National Institute of Standards and Technology, Gaithersburg, MD 20899-6102, United States

[‡]National Renewable Energy Laboratory, Golden, CO 80401, United States

[§]Laboratoire de Réactivité et Chimie des Solides (LRCS), UMR 7314 CNRS, Université de Picardie Jules Verne, 33 rue Saint-Leu, 80039 Amiens Cedex, France

[‡]Department of Materials Science and Engineering, University of Maryland, College Park, MD 20742-2115, United States

^ΔGeophysical Laboratory, Carnegie Institution of Washington, Washington, DC 20015, United States

[#]Institute of Metal Physics, Ural Branch of the Russian Academy of Sciences, Ekaterinburg, 620108, Russia

ABSTRACT:

Quasielastic neutron scattering (QENS) measurements over a wide range of energy resolutions were used to probe the reorientational behavior of the pyramidal SiH_3^- anions in the mono-alkali silanides (MSiH_3 , where $M = \text{K}, \text{Rb},$ and Cs) within the low-temperature ordered β -phases, and for CsSiH_3 , the high-temperature disordered α -phase and intervening hysteretic transition region. Maximum jump frequencies of the β -phase anions near the β - α transitions range from around 10^9 s^{-1} for β - KSiH_3 to 10^{10} s^{-1} and higher for β - RbSiH_3 and β - CsSiH_3 . The β -phase anions undergo uniaxial three-fold rotational jumps around the anion quasi- C_3 symmetry axis. CsSiH_3 was the focus of further studies to map out the evolving anion dynamical behavior at temperatures above the β -phase region. As in α - KSiH_3 and α - RbSiH_3 , the highly mobile anions (with reorientational jump frequencies approaching and exceeding 10^{12} s^{-1}) in the disordered α - CsSiH_3 are all adequately modeled by H jumps between 24 different locations distributed radially around the anion center of gravity, although even higher anion reorientational disorder cannot be ruled out. QENS data for CsSiH_3 in the transition region between the α - and β -phases corroborated the presence of dynamically distinct intermediate (i -) phases. The SiH_3^- anions within these i -phases appear to undergo uniaxial small-angular-jump reorientations that are more akin to the lower-dimensional β -phase anion motions rather than to the multi-dimensional α -phase anion motions. Moreover, they possess orientational mobilities that are an order-of-magnitude lower than those for α -phase anions but also an order-of-magnitude higher than those for β -phase anions. Combined QENS and neutron powder diffraction results strongly suggest that this i -phase is associated chiefly with the more short-range-ordered, nanocrystalline portions (invisible to diffraction) that appear to dominate the CsSiH_3 .

Introduction

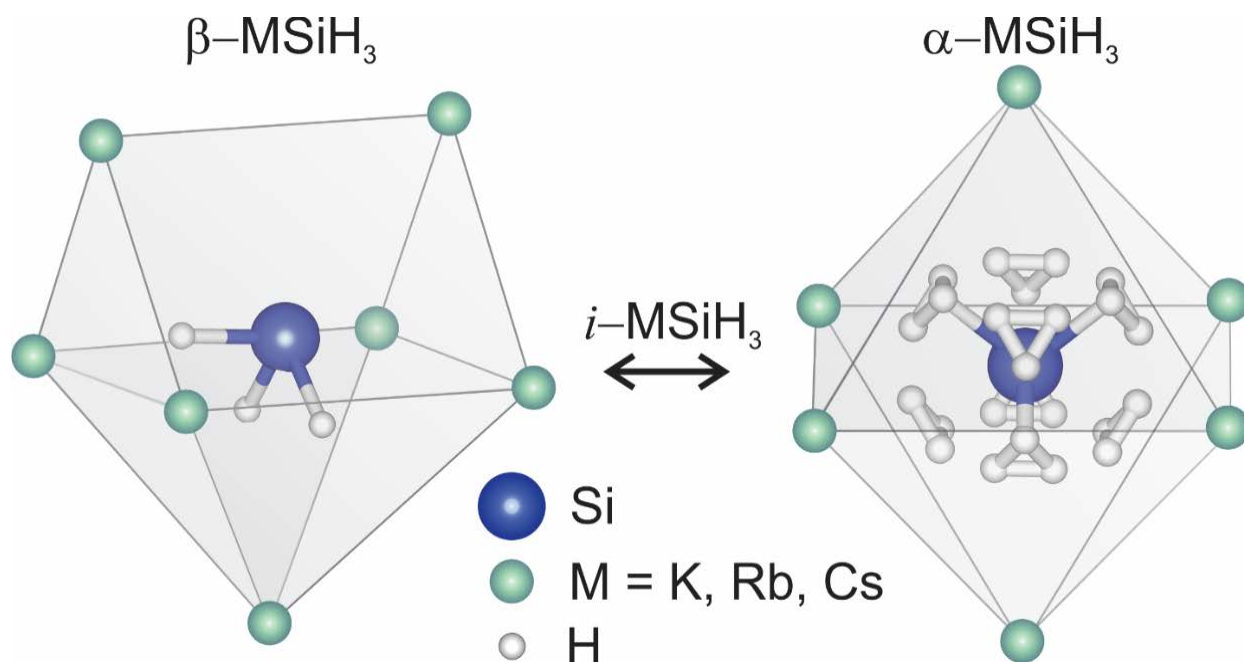


Figure 1. Structural differences between the ordered β -MSiH₃ and disordered α -MSiH₃ (M = K, Rb, Cs) phases showing the respective near-neighbor cation environments (7-coordination for the former and 6-coordination for the latter). M⁺ alkali metal cations are denoted by green spheres, whereas the pyramidal SiH₃⁻ anions are denoted by blue Si spheres and white H spheres. N.B., although one specific anion orientation is highlighted in α -MSiH₃, the multiple H atoms distributed radially around the Si atom represent all of the possible H positions associated with the orientationally disordered SiH₃⁻ anions in this structure. N.B., i -MSiH₃ is meant to be a general term to denote the possible formation of ‘intermediate’ phases in the transition regions with intermediate SiH₃⁻ anion orientational mobilities between those for the β -MSiH₃ and α -MSiH₃ phases.

Alkali-metal silanides (MSiH₃, M = K, Rb, and Cs) have recently gained attention as potential hydrogen-storage compounds due to their reversible dehydrogenation/ hydrogenation properties.^{1,2,3,4,5} Typically, a silanide ↔ silicide equilibrium (i.e., MSiH₃ ↔ MSi + 1.5H₂) exists, providing favorable hydrogen vapor pressures of 0.1 MPa near 410 K.³ All MSiH₃ compounds studied, including the various alkali-metal-alloy versions (K_{0.5}Cs_{0.5}SiH₃, K_{0.5}Rb_{0.5}SiH₃, and Rb_{0.5}Cs_{0.5}SiH₃) undergo hysteretic phase transitions upon heating and cooling between ordered monoclinic or orthorhombic β -phase structures to disordered face-centered-cubic α -phase

structures^{3,6,7,8,9} (see Figure 1). In contrast to the crystallographically ordered, β -phase SiH_3^- anions, the α -phase anions exhibit three-dimensional orientational disorder. Neutron scattering fixed-window-scans (FWSs)⁹ and differential scanning calorimetry/heat capacity measurements^{3,10} in heating and cooling regimens confirm that the transitions between α - MSiH_3 and β - MSiH_3 phases are highly hysteretic.

An NMR wide-line investigation,⁷ as well as neutron total scattering and infrared, Raman, and neutron vibrational spectroscopy measurements in conjunction with density functional theory calculations^{11,12} suggested that this α -phase anion disorder was dynamical in nature. Subsequent quasielastic neutron scattering (QENS) measurements of the α - MSiH_3 phases^{9,13} confirmed rapid reorientational mobilities ($>10^{12}$ small-angular jumps s^{-1}) for the orientationally disordered SiH_3^- anions above room temperature. The momentum-transfer dependence of the quasielastic scattering was typically consistent with a three-dimensional reorientational jump mechanism in which the three H atoms of each rigid-body SiH_3^- anion traverse the surface of a sphere that is roughly centered on the Si atom. The QENS data were more in accordance with reorientational jumps between multiple yet discrete H positions (being successfully modelled as jumps among the 24 different, neutron-powder-diffraction-derived, crystallographic H positions previously used to describe the orientational disorder³) rather than fully isotropic (random walk) rotational diffusion.

Additional FWS measurements for all mono-alkali and di-alkali-metal silanides have indicated orders-of-magnitude lower anion orientational mobilities in the ordered β -phases,⁹ a finding in general agreement with subsequent Raman, heat capacity, and ^2H NMR investigations of $\text{KSi}(\text{H}/\text{D})_3$ and $\text{RbSi}(\text{H}/\text{D})_3$.¹⁰ Interestingly, these and other QENS data showed that the anion mobility in the β -phase mono-alkali silanides trended higher with increasing alkali-metal-cation size, whereas the opposite trend was observed in the α -phases.^{9,13} Moreover, in contrast to the

highly disordered α -phases, the single crystallographic orientations for each SiH_3^- anion in the ordered β -phases point to only one physically reasonable β -phase reorientational mechanism, i.e., uniaxial three-fold rotational jumps of the H atoms around the anion's nominal C_3 symmetry axis.

A recent study by Nedumkandathil *et al.*¹⁰ focusing on the order-disorder rotator-phase transition in KSiH_3 and RbSiH_3 used ^2H NMR to show that presumably nanosized (2-4 nm) disordered α -like domains persisted well below the α -phase to β -phase transition temperature delineated by heat capacity measurements upon cooling. Moreover, QENS data suggested that these α -like nanodomains possess a markedly reduced SiH_3^- anion orientational mobility, with significantly longer relaxation times on the order of picoseconds instead of the 0.2-0.3 ps between reorientational jumps observed for bulk α -phase above the phase transition. It was surmised that a rather weak coordination of SiH_3^- anions among the alkali metal cations was the cause of such lingering disordered subcooled nanophases.

In the current paper, high-resolution QENS measurements are used to fully characterize the alkali-metal-dependent anion reorientational dynamics in three β - MSiH_3 compounds (M= K, Rb, and Cs) as well as the unusual nature of the rotator-phase transition between the β -phases and α -phases for CsSiH_3 . These QENS results bolster the general conclusion of the previous NMR/QENS study¹⁰ that distinct subcooled intermediate phases exist and exhibit anion orientational mobilities intermediate between those for the α -phases and β -phases. The suggested nature of the SiH_3^- anion reorientations in the intermediate CsSiH_3 phase also points to an *intermediate mechanistic* behavior to those for the α -phase and β -phase. Complementary temperature-dependent neutron powder diffraction (NPD) measurements for CsSiD_3 lead us to conclude that this intermediate phase is associated with the significant fraction of nanosized crystallites presumably present in the material.

Experimental Details

MSi (M = K, Rb, and Cs) alloys of the order of 1 g each were synthesized by high-temperature annealing of 1:1.03 atomic ratios of metal to silicon, using potassium (99.95%, Sigma-Aldrich¹⁴), rubidium (99.75%, Alfa Aesar), cesium (99.8%, Alfa Aesar), and silicon (powder, –325 mesh Sigma-Aldrich) starting materials. All materials were handled in an argon-filled glovebox. Each mixture was arc-weld-sealed within a stainless-steel ampule inside the glovebox. The ampules were typically heated 1 K min^{-1} from room temperature to 773 K for KSi, and to 873 K for all other alloys, holding them for 48 h before cooling 0.2 K min^{-1} back down to room temperature. A slight excess of silicon was added to ensure that all the starting alkali metals were reacted. All resulting MSi samples were first activated via evacuation at 473 K for 12 h and then hydrogenated at 373 K with ca. 5 MPa of hydrogen for up to 24 h. An additional, deuterated CsSiD₃ sample for NPD measurements was synthesized in the same fashion and was the same material used in [Ref. 3](#).

Quasielastic neutron scattering measurements were performed at the National Institute of Standards and Technology (NIST) Center for Neutron Research (NCNR) on the Disk Chopper Spectrometer (DCS),¹⁵ High-Flux Backscattering Spectrometer (HFBS),¹⁶ and NGA Neutron Spin Echo Spectrometer (NSE).¹⁷ DCS measurements utilized incident neutron wavelengths of 2.75 Å (10.8 meV), 4.8 Å (3.55 meV), 6 Å (2.27 meV), and 8 Å (1.28 meV) with respective resolutions of 275 μeV , 56 μeV , 30 μeV , and 30 μeV full width at half maximum (fwhm) and respective maximum attainable Q values of around 4.30 \AA^{-1} , 2.46 \AA^{-1} , 1.98 \AA^{-1} , and 1.48 \AA^{-1} . The instrumental resolution function was determined from the measured QENS spectrum at 25 K in all cases. The measurements were performed on CsSiH₃ at multiple temperatures in the range from 170 K to 350 K, in both heating and cooling regimens. Additional corroborating measurements

were performed on RbSiH₃ at 281 K after cooling from 300 K. HFBS measurements utilized an incident neutron wavelength of 6.27 Å, yielding a resolution of 0.8 μeV fwhm. QENS measurements on the HFBS spectrometer were performed on CsSiH₃, RbSiH₃, and KSiH₃ in the temperature range from 150 K to 300 K. The instrumental resolution function was determined from the measured QENS spectrum at 4 K. NSE measurements were performed on CsSiH₃ at 140 K (and at 4 K for the resolution) utilizing an incident neutron wavelength of 6.0 Å at (2.27 meV, $\Delta\lambda/\lambda \approx 0.18$) for Fourier times up to 17.5 ns at $Q = 0.8 \text{ \AA}^{-1}$. NPD measurements on CsSiD₃ were performed at the Institut Laue Langevin (ILL, Grenoble, France) on the D1B diffractometer ($\lambda = 1.289 \text{ \AA}$).

Data were analyzed using Mslice and PAN programs within the DAVE software package.¹⁸ Standard uncertainties in all figures in the text and supporting information (SI), if not explicitly indicated, are commensurate with the observed scatter in the data.

Results and Discussion

MSiH₃ β -phase Dynamics

Figure S1 in the SI illustrates neutron FWS data for MSiH₃ (M = K, Rb, and Cs), adapted from Ref. 9, upon both heating and cooling regimens, which reveals the significant hystereses in SiH₃⁻ orientational mobilities reflecting the hysteretic phase change behaviors for these compounds. Thus, it is important to emphasize that the relative fractions of compound phases present at any particular temperature depends strongly on the temperature history. Since the FWSs indicate considerably low SiH₃⁻ orientational mobilities for the various β -MSiH₃ phases, these particular mobilities could only be practically probed using the two highest-resolution

spectrometers, namely HFBS and NSE, during heating regimens from low to high temperatures which ensure higher hysteretic β - α phase boundary temperatures.

Representative QENS spectra of β -KSiH₃, β -RbSiH₃, and β -CsSiH₃ at Q values of 1.16 Å⁻¹ obtained on the HFBS spectrometer and measured at temperatures of 292 K, 260 K, and 200 K, respectively, are shown in [Figure 2](#). In all cases, the spectra were fit with a delta function (elastic scattering) and one Lorentzian function, both convoluted with the instrumental resolution function, above a flat background. Indeed, the constant Q -dependences of the quasielastic linewidths obtained for all compounds ([Figure 3](#)) are consistent with the three-site jump model,¹⁹ which is expected for the β -phase and in which H atoms are reorienting by 120° jumps about the nominal three-fold symmetry axis of the SiH₃⁻ group. Again, we stress that such a model is dictated by the ordered crystallographic structures of the β -phases, which restricts the possible H positions to three locations around the directionally invariant, anion C_3 axis.

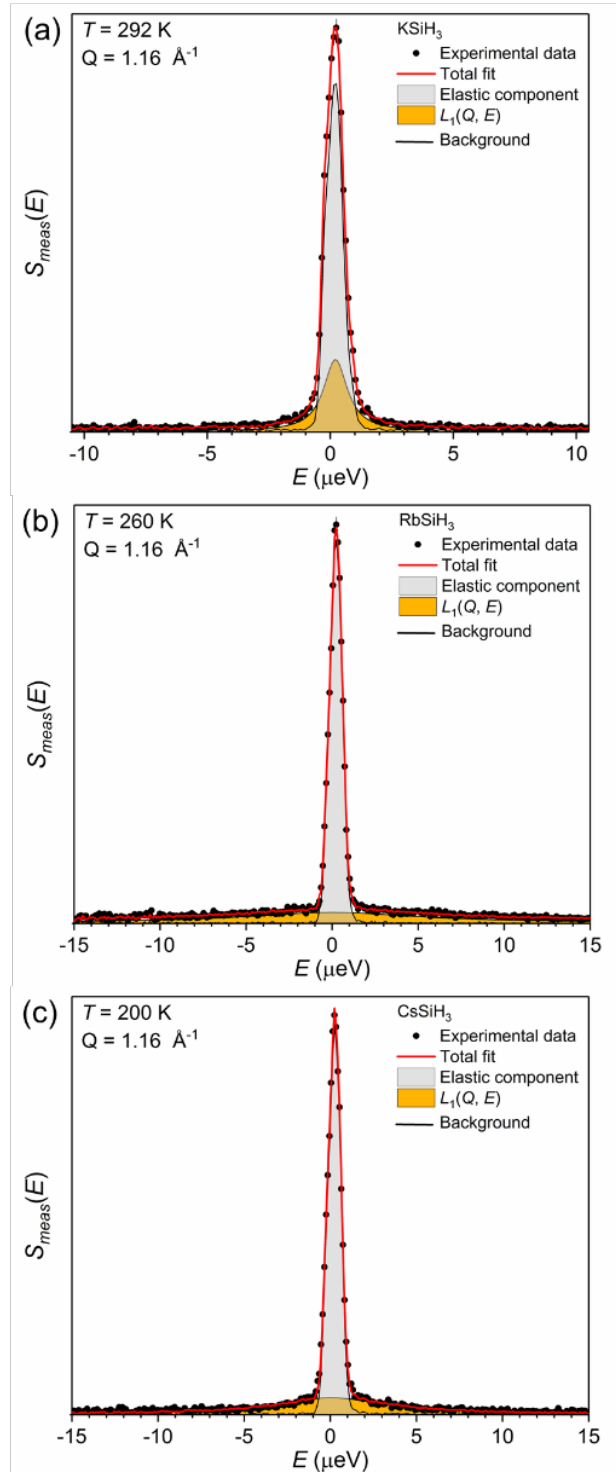


Figure 2. Exemplary QENS spectra of (a) β -KSiH₃, (b) β -RbSiH₃ and (c) β -CsSiH₃ at Q values of 1.16 \AA^{-1} obtained on the HFBS spectrometer and measured at temperatures of 292 K, 260 K, and 200 K, respectively. Spectra were fit with a delta function and one Lorentzian component, both convoluted with the instrumental resolution function, on top of a flat background.

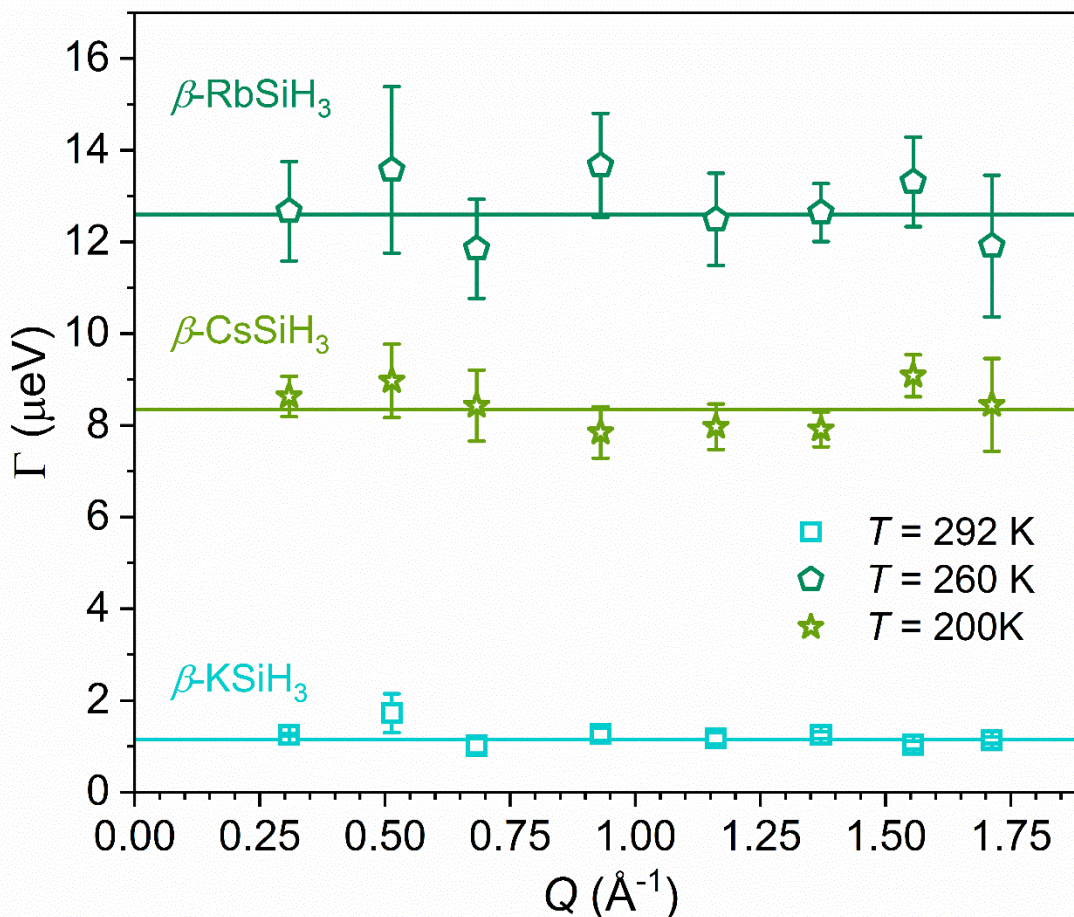


Figure 3. Q -dependence of the Lorentzian (quasielastic) fwhm linewidths for β -KSiH₃, β -RbSiH₃, and β -CsSiH₃ obtained on the HFBS spectrometer and measured at temperatures of 292 K, 260 K, and 200 K, respectively.

Table 1. Comparison of Activation Energies for Reorientations Determined from QENS Data

Compound	QENS activation energy (meV)	Compound	QENS activation energy (meV)
α -KSiH ₃	39(1) ¹³	β -KSiH ₃	160(2) 517(3) ^a
α -RbSiH ₃	33(1) ¹³	β -RbSiH ₃	190(2)
α -CsSiH ₃	48(2) 32(3) ⁹	β -CsSiH ₃	105(2)

^a This fitted value is based on an additional assumed τ_1^{-1} value of 10^5 s^{-1} at 200 K estimated from NMR data from Ref. 10.

Figure 4 illustrates the temperature-dependent linewidths for the β -phase compounds plotted in an Arrhenius fashion. The fundamental jump correlation frequencies τ_1^{-1} are calculated from the Lorentzian fwhm linewidths Γ by $\tau_1^{-1} = \Gamma/(2\hbar)$. The slope of $\ln(\tau_1^{-1})$ vs. T^{-1} is $-E_a/k_B$, where E_a is the activation energy for anion reorientation and k_B is the Boltzmann constant. For β -CsSiH₃, QENS measurements were extended further down in temperature to 140 K using the NSE spectrometer (see Figure S2 for data and analysis). Table 1 lists fitted E_a values of 160(2) meV, 190(2) meV, and 105(2) meV for β -KSiH₃, β -RbSiH₃, and β -CsSiH₃, respectively. At first glance, there appears to be no monotonic trend between E_a and unit cell size, contrary to what one might expect based on previous reports of similar local seven-fold alkali-metal-cation coordination environments surrounding each β -phase SiH₃⁻ anion. One caveat is that, due to the specific details of β -KSiH₃ phase behavior and particularly low associated anion mobility, we are only able to assess a rather limited 20 K temperature range (280 K to 300 K) for this compound. This leads to more uncertainty in the fitted E_a value. In fact, solid-state ²H NMR spectroscopic results for β -KSiD₃ (Ref. 10) suggest to us anion reorientational jump frequencies of roughly the order of 10⁵ s⁻¹ by 200 K based on the temperature dependence of the ²H NMR spectra. Inclusion of this extra data point in our analysis (see Figure 4) would lead to a much higher fitted E_a value of 517(3) meV. Yet, we note that the 200 K jump frequency for the lighter H-isotope β -KSiH₃ is likely somewhat higher due to the higher expected torsional attempt frequency (*e.g.*, by a factor of $\sqrt{2}$ in the harmonic case) for H vs D. Nonetheless, even if we assume a ten-fold-larger τ_1^{-1} value at 200 K for β -KSiH₃, this would still yield a larger E_a value [383(3) meV] than for β -RbSiH₃. Hence it is not unreasonable to assume that a trend does actually exist between E_a and unit cell size, with both lower anion mobilities and higher activation energy barriers resulting in general from smaller, more sterically restrictive anion sites. In contrast to the comparatively similar anion

mobilities reported for all three different α -phase compounds,^{9,13} the trending differences in anion mobilities between β -phase compounds are particularly dramatic, as exemplified in Figure 4 by the two-orders-of-magnitude less mobile anions in β -KSiH₃ compared to those in β -CsSiH₃ extrapolated to the same temperatures.

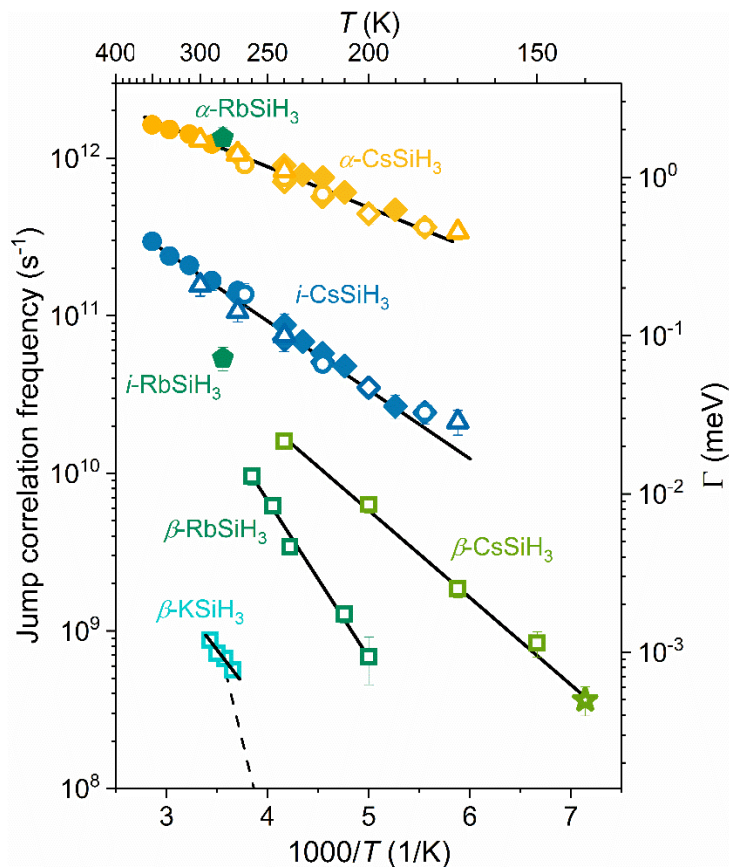


Figure 4. Anion jump correlation frequencies τ_1^{-1} vs. $1/T$ for various KSiH₃, RbSiH₃, and CsSiH₃ phases plotted in an Arrhenius fashion as determined from measurements on DCS, HFBS, and NSE spectrometers. DCS measurements were performed with neutron wavelengths of 2.75 Å (circles), 4.8 Å (diamonds), 6 Å (triangles), and 8 Å (pentagons) with respective fwhm resolutions of 275 μ eV, 56 μ eV, 30 μ eV, and 30 μ eV. HFBS measurements are presented by squares, obtained with 6.27 Å wavelength neutrons with a fwhm resolution of 0.8 μ eV. The NSE measurement (star) was obtained with 6.0 Å wavelength neutrons. Filled and open symbols indicate measurements during cooling and heating regimens, respectively. The dashed line for β -KSiH₃ represents the linear fit obtained upon inclusion of an anion reorientational jump frequency of 10^5 s⁻¹ at 200 K estimated from prior NMR measurements.¹⁰

While we make this comparison, it is worth mentioning that the most recent neutron powder diffraction patterns¹⁰ following the structural evolution of β -KSiD₃ and β -RbSiD₃ with increasing temperature suggested that the latter compound begins distorting slightly from its original low-temperature monoclinic structure with increasing temperature starting somewhere above 200 K to 210 K. By 240 K a triclinically distorted β -RbSiD₃ structure appeared to provide a better fit to the data before further transformation to the α -phase at higher temperature. This proposed triclinic transformation was bolstered by complementary NMR, Raman, and heat capacity measurements.¹⁰ In contrast, β -KSiD₃ did not seem to deviate from its low-temperature orthorhombic structure, and there was no further comparative study undertaken for β -CsSiD₃. Based on this information, we cannot rule out that a progressive triclinic distortion with increasing temperature, although minor, is noticeably affecting the corresponding SiH₃⁻ mobilities and reorientational barriers determined from the β -RbSiH₃ QENS results (and possibly even the β -CsSiH₃ results).

There is general agreement between the β -phase results in [Figure 4](#) and the FWSs in [Figure S1](#). Anion reorientational jump frequencies reach about 10^8 s^{-1} by around 250 K, 175 K, and 125 K for β -KSiH₃, β -RbSiH₃, and β -CsSiH₃, respectively. (N.B., we previously quoted somewhat lower respective temperatures of $\sim 225 \text{ K}$, 150 K , and 80 K based on the observed earliest onset of accelerating FWS intensity loss,⁹ but it is clear now that these estimated threshold points more accurately reflected slightly smaller τ_1^{-1} values somewhere between 10^7 and 10^8 s^{-1} .) At the higher temperatures, in contrast with β -KSiH₃, which never attains reorientational jump frequencies above $\approx 10^9 \text{ s}^{-1}$ before transformation to the α -phase, β -RbSiH₃ and β -CsSiH₃ respectively reach and exceed 10^{10} s^{-1} by the time they undergo their β - α transformations. Therefore, the FWS intensities for the latter two clearly begin plateauing out (which reflects the

quasielastic component widths becoming too overly broad and disappearing into the flat HFBS baseline scattering) during heating regimens on approach to their α -phases, whereas the corresponding FWS intensity for β -KSiH₃ continues dropping within the 10⁸-10¹⁰ s⁻¹ frequency window of the spectrometer until it suddenly and more steeply collapses further toward its lower α -phase plateau, like the other two congeners. This universal drop to a lower α -phase plateau simply reflects an increase in the expected fraction of quasielastic scattering due to the transition in SiH₃⁻ reorientational mechanism from β -phase uniaxial reorientations to α -phase three-dimensional sphere-tracing reorientations.

CsSiH₃ α -phase and Transition-Region Dynamics

In comparison to the β -phases, the α -phases exhibit orders-of-magnitude-higher anion orientational mobilities. From an experimental viewpoint, it is apparent that α -CsSiH₃ is the best of the three α -phase silanides to investigate because it provides the widest temperature range accessible within the neutron scattering resolution windows of our instruments. Thus, to gain more insights into SiH₃⁻ dynamics in the α -phases and the nature of the rotator-phase transition, we focused our attention on α -CsSiH₃ as well as the hysteretic transformations between α -CsSiH₃ and β -CsSiH₃.

Figure 5 illustrates T -dependent QENS spectra of α -CsSiH₃ measured on the DCS spectrometer at Q values of 1.20 and 2.20 Å⁻¹ and temperatures of 270 K and 240 K attained upon cooling from 350 K. In line with prior results for α -KSiH₃, α -RbSiH₃, and α -CsSiH₃,^{9,10,13} the QENS spectra were initially fit with a resolution-convoluted lineshape comprised of one elastic component (delta function) together with two Lorentzian functions. However, the higher-resolution measurements with wavelengths of 4.8 Å and 6 Å clearly indicated the need for

inclusion of an additional narrower Lorentzian component. Thus, a reasonable spectral fit required three Lorentzian components with order-of-magnitude-different widths, in addition to an elastic peak component and a flat background. The two narrower Lorentzian components are associated with quasielastic scattering from SiH_3^- anion reorientations, while the very broad Lorentzian is consistent with low-energy inelastic scattering from overdamped anion vibrational modes, as observed previously for QENS measurements of α - KSiH_3 , α - RbSiH_3 , and α - CsSiH_3 ,^{9,10,13} as well as for other systems with highly mobile anions such as the disordered Li and Na decahydro-*closo*-deca(carba)borate salts.²⁰ This is further confirmed by the $Q^2 \exp(-Q^2 \langle u^2 \rangle)$ dependence of the intensity, where $\langle u^2 \rangle$ is the mean-squared displacement and $\exp(-Q^2 \langle u^2 \rangle)$ is the Debye-Waller factor, which is in line with the expected behavior for the scattering intensity of an overdamped vibrational feature (see Figure S3). The fitted root-mean-squared H displacement for this feature was 0.38(3) Å, which one can interpret as the rough oscillatory distance travelled by the H atoms within localized wells comprising the corrugated rotational potential landscape, distinct from the longer-distance, much-lower-frequency H rotational jumps between these wells leading to the quasielastic scattering components.

Figure 6 presents the Q -dependences of the quasielastic linewidths of the two narrower Lorentzian components of α - CsSiH_3 measured at 270 K. The increasing linewidth of the broader component with Q above about 1.5 Å⁻¹ indicates similar behavior to what was previously observed for α - KSiH_3 and α - RbSiH_3 ,¹³ and signals a small-angle jump-diffusion mechanism with fundamental jump correlation frequencies τ_1^{-1} of the order of 10¹¹ to 10¹² s⁻¹, which is in the expected range of anion mobilities in the α -phase.

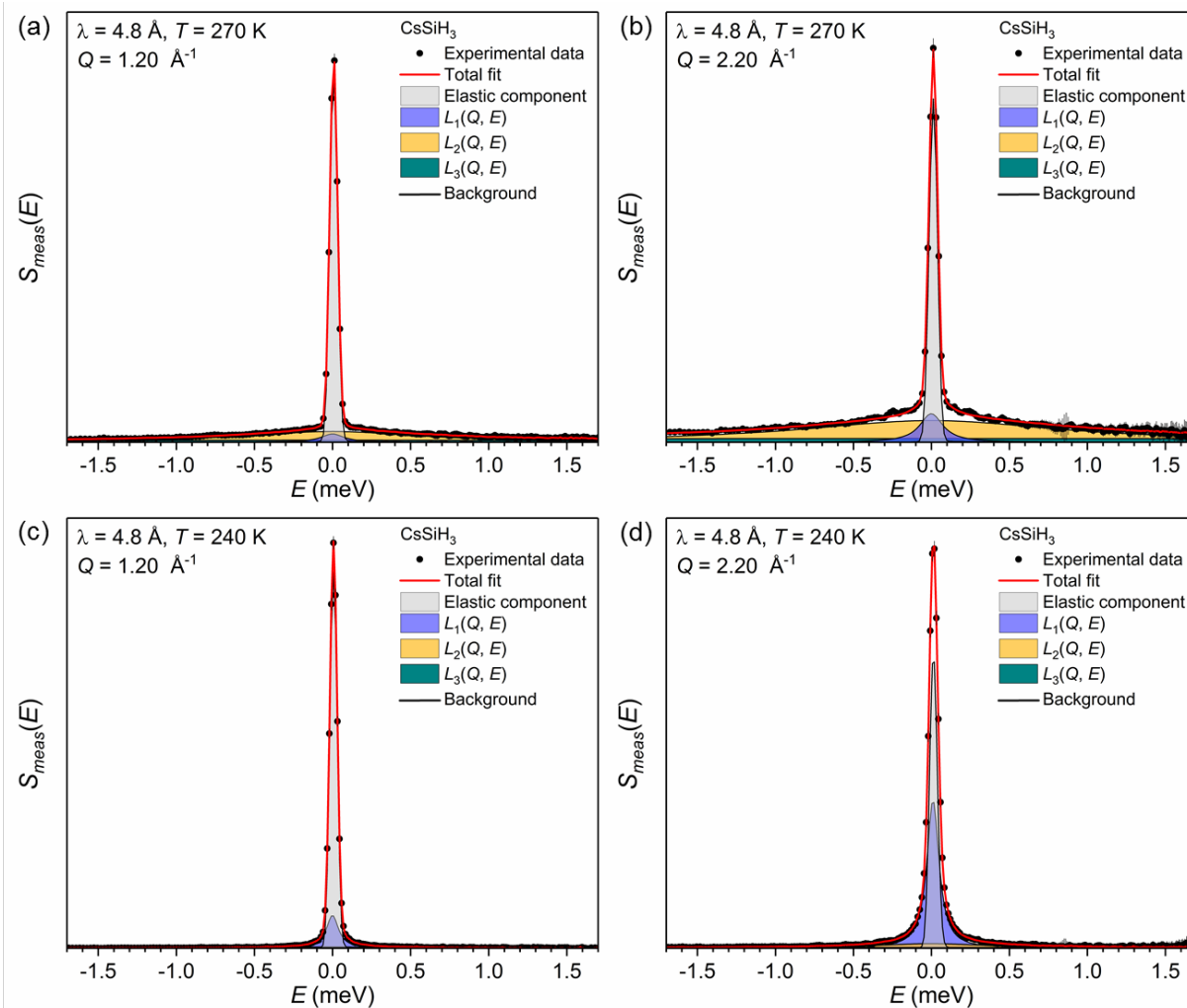


Figure 5. Exemplary QENS spectra for CsSiH₃ (in cooling) at 270 K ((a) $Q = 1.20 \text{ \AA}^{-1}$ and (b) $Q = 2.20 \text{ \AA}^{-1}$) and 240 K ((c) $Q = 1.20 \text{ \AA}^{-1}$ and (d) $Q = 2.20 \text{ \AA}^{-1}$) using 4.8 \AA wavelength neutrons (with 56 μeV fwhm resolution). Spectra were fit with a delta function and three Lorentzian components, all four convoluted with the instrumental resolution function, on top of a flat background.

Although the second Lorentzian component is almost an order of magnitude narrower than the broader bulk α -phase component discussed above, it is still almost an order of magnitude broader than the quasielastic CsSiH₃ component found earlier for the β -CsSiH₃ phase, so it presumably marks the presence of a third dynamically distinctive phase. The relatively constant linewidth with increasing Q for this component in Figure 6 compared to that for the α -phase suggests an anion reorientational mechanism more in accord with a uniaxial H jump mechanism as for β -phase SiH₃⁻

anions, but of much higher mobility. For lack of a better term, we refer to this coexisting “intermediate” phase as the *i*-phase.

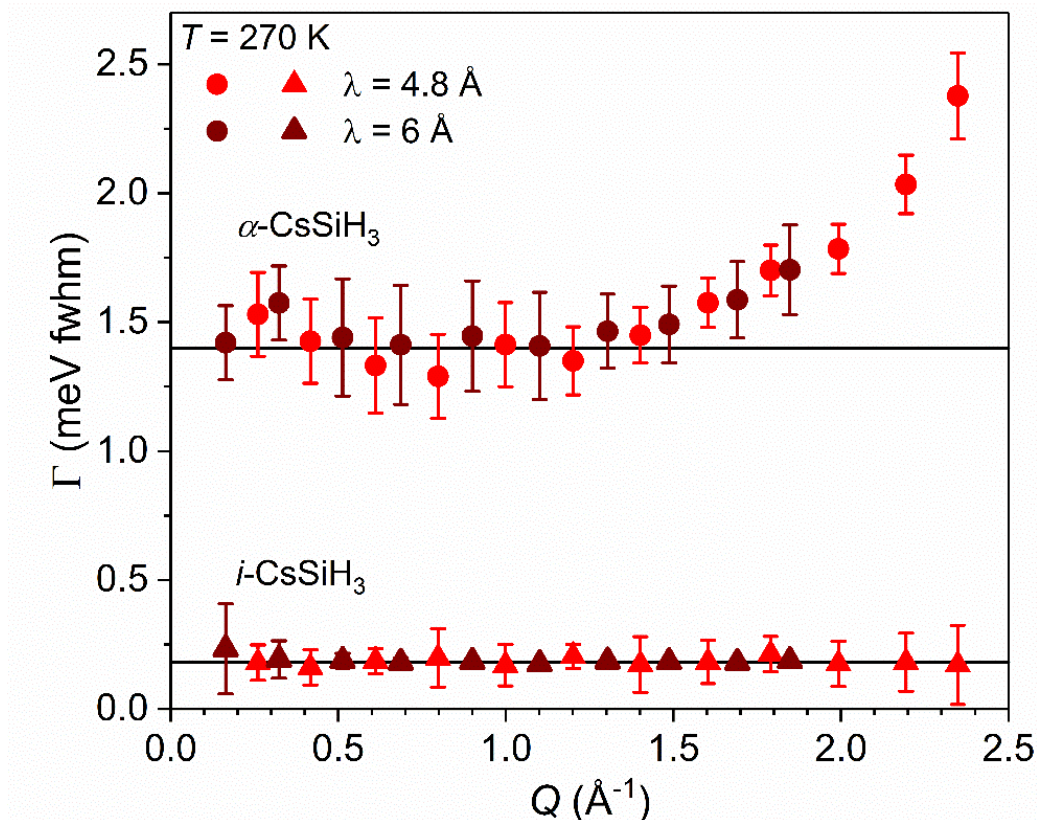


Figure 6. Q -dependence of the two narrower Lorentzian (quasielastic) fwhm linewidths Γ for CsSiH_3 (in cooling) at 270 K measured with 4.8 Å (red symbols) and 6.0 Å (dark red symbols) wavelength neutrons with respective fwhm resolutions of 56 μeV and 30 μeV .

Figure 4 includes the Arrhenius-type plots for τ_1^{-1} (and corresponding linewidths) for the α - and i -phases of CsSiH_3 during both heating and cooling regimens. For the α -phases, the average linewidths were calculated for Q values $< 1.5 \text{ \AA}^{-1}$ (the flat region in Figure 6). For the i -phases (as for the β -phases), the averaging of linewidths included all Q values.

The τ_1^{-1} data indicate SiH_3^- anion reorientational jump frequencies for disordered α - CsSiH_3 between around $3 \times 10^{11} \text{ s}^{-1}$ and $2 \times 10^{12} \text{ s}^{-1}$, in accordance with the prior QENS results.^{9,10,13} This is in contrast to the much less mobile anions in the ordered β -phases for all compounds, almost two

order of magnitudes slower in comparison to the α -phase, leaving them in the range from 2×10^8 s⁻¹ to 1×10^{10} s⁻¹. The much lower anion mobility in the ordered β -phases compared to the disordered α -phases is expected, due to the smaller (more sterically restrictive) unit cell volume for the former. The τ_1^{-1} values for *i*-CsSiH₃ are clearly intermediate between those for the α - and β -phases, ranging from around 2×10^{10} s⁻¹ to 3×10^{11} s⁻¹. The temperature dependences of the *i*-CsSiH₃ and α -CsSiH₃ τ_1^{-1} values in [Figure 4](#) are found to be largely unaffected by thermal history, even if their relative phase fractions (as determined by the QENS data) may differ somewhat between heating and cooling regimens. This varies somewhat from the behavior that was previously reported for the “undercooled α -phases” for KSiH₃ and RbSiH₃,¹⁰ where there were order-of-magnitude differences in effective τ_1^{-1} values depending on whether these phases were “remnant” (i.e., remaining upon cooling down from the α -phases) or “premonitory” (i.e., appearing upon heating up from the β -phases). Hence, it is possible that the details of the structural and dynamical evolution in the transition region for CsSiH₃ are somewhat different than those seen for KSiH₃ and RbSiH₃.

The simplest picture in agreement with our CsSiH₃ results points to the temperature-dependent formation of three dynamically distinct phases (β -CsSiH₃, *i*-CsSiH₃, and α -CsSiH₃). Unlike for KSiH₃ and RbSiH₃,¹⁰ SiH₃⁻ reorientational mobilities for undercooled α -CsSiH₃, designated as remnant (i.e., α -phase below the approximate 250 K $\alpha \rightarrow \beta$ phase transition temperature upon cooling) and premonitory (i.e., α -phase below the approximate 310 K $\beta \rightarrow \alpha$ phase transition temperature upon heating) according to the nomenclature from [Ref. 10](#), show no deviations from the expected temperature-dependent bulk α -phase mobilities. This makes sense, since anion mobilities are mainly dictated by the local details of their near-neighbor environment. If the local structure of bulk α -phase is present in the undercooled region, either as a few unit cells

or as large crystallites, the associated anion dynamics will be the same. Without further corroborating structural information, one might be tempted to label the *i*-CsSiH₃ phase itself as an undercooled α -phase (i.e., with a reduced local cubic unit cell constant but nano-crystalline and invisible to diffraction), although again (unlike for KSiH₃ and RbSiH₃),¹⁰ there is no distinction found between remnant and premonitory SiH₃⁻ anion mobilities. Alternatively, *i*-CsSiH₃ might represent a different more coarsely crystalline intermediate phase, maybe even analogous to the reported intermediate triclinic β' -RbSiH₃ phase,¹⁰ although the intermediate anion mobility would again certainly require a structure with an intermediate unit cell volume. We will assess these possibilities later in the paper based on temperature-dependent NPD measurements of CsSiD₃.

To see if there was also some analogous intermediate dynamic present for another silanide besides CsSiH₃, we performed one high-resolution (30 μ eV fwhm) QENS measurement on RbSiH₃ on the DCS spectrometer at 281 K, after cooling α -RbSiH₃ from 300 K. Again, a reasonable spectral fit required two Lorentzian components with order-of-magnitude-different widths in addition to an elastic peak component and a flat background, which already adequately included the very broad overdamped phonon scattering over the limited energy range considered. (See [Figure S5](#)), Based on the calculated fundamental jump correlation frequencies τ_1^{-1} for these two components, it was evident that the dominant broader Lorentzian component yielding a higher τ_1^{-1} value of the order 10^{12} s⁻¹ was reflective of bulk α -RbSiH₃.^{10,13} On the other hand, a τ_1^{-1} value of the order 5×10^{10} s⁻¹ corresponding to the narrower Lorentzian component (which was roughly 10 % as intense as the broader component) was again too large to be attributed to the β -RbSiH₃ phase and thus must correspond to some type of unknown intermediate structural arrangement. The two τ_1^{-1} values are plotted with the CsSiH₃ data in [Figure 4](#). Noting the fairly close proximity of the jump correlation frequency for the intermediate phase to an extrapolation of the jump

frequencies for the β -RbSiH₃ phase in Figure 4, we speculate that it may be reflecting the presence of some small fraction of β -like triclinic β' -RbSiH₃ phase, although there is no structural or other evidence supporting its presence upon cooling α -RbSiH₃ from 300 K. In light of the results of this intriguing RbSiH₃ measurement and the lack of any other comparable high-resolution QENS measurements, it would likely be worthwhile to perform more detailed high-resolution QENS experiments in the future on both KSiH₃ and RbSiH₃ in the transitional temperature region to more fully map out the behavior of any such lower-mobility species.

The activation energies E_a obtained from the slopes of the linear fits in Figure 4 are presented in Table 1. The E_a values of 39(1) meV, 33(1) meV, and 32(3) meV, respectively, for the three α -MSiH₃ (M = K, Rb, and Cs) phases reported previously from Refs. 9 and 13 were determined by ignoring any potential additional “contamination” broadening from a narrower i -phase-related Lorentzian component. This may or may not be so consequential for α -KSiH₃ or α -RbSiH₃, but for the current higher-resolution α -CsSiH₃ data in Figure 4, the inclusion of a second i -phase-related component in the analysis results in a 50 % higher E_a value of 48(2) meV.

The QENS data for i -CsSiH₃ in Figure 4 led to a fitted E_a value of 89(2) meV, which lies between the corresponding values of 105(2) meV and 48(2) meV for the respective β -CsSiH₃ and α -CsSiH₃ phases. The intermediate values for both activation energies and anion reorientational jump frequencies are reasonable from a steric viewpoint if the i -phase actually possesses a unit-cell volume per MSiH₃ formula unit that is intermediate between those for the β -CsSiH₃ and α -CsSiH₃ phases. Of course, confirming such structural details with any diffraction-based probe would require the i -phase to attain adequately large crystallite domain sizes, which is a topic again assessed later in the paper in light of our NPD measurements. Yet, even without structural measurements, we show in the next section that a comparison of the corresponding SiH₃⁻

reorientational mechanisms proposed from QENS measurements for the three different phases can provide further insights concerning the nature of the *i*-phase.

Anion Reorientational Mechanisms

Mechanistic insights concerning the SiH_3^- reorientational dynamics associated with the different phases of these compounds can be deduced from the Q -dependence of the relative fractions of elastic and quasielastic scattering intensities. This information is typically conveyed by the elastic incoherent structure factor (EISF), which is defined at any Q value as the ratio of elastic to total (elastic+quasielastic) scattering intensities. [Figure 7](#) compares the experimental EISF values with hypothetical curves derived for various different SiH_3^- reorientation models detailed in the SI.

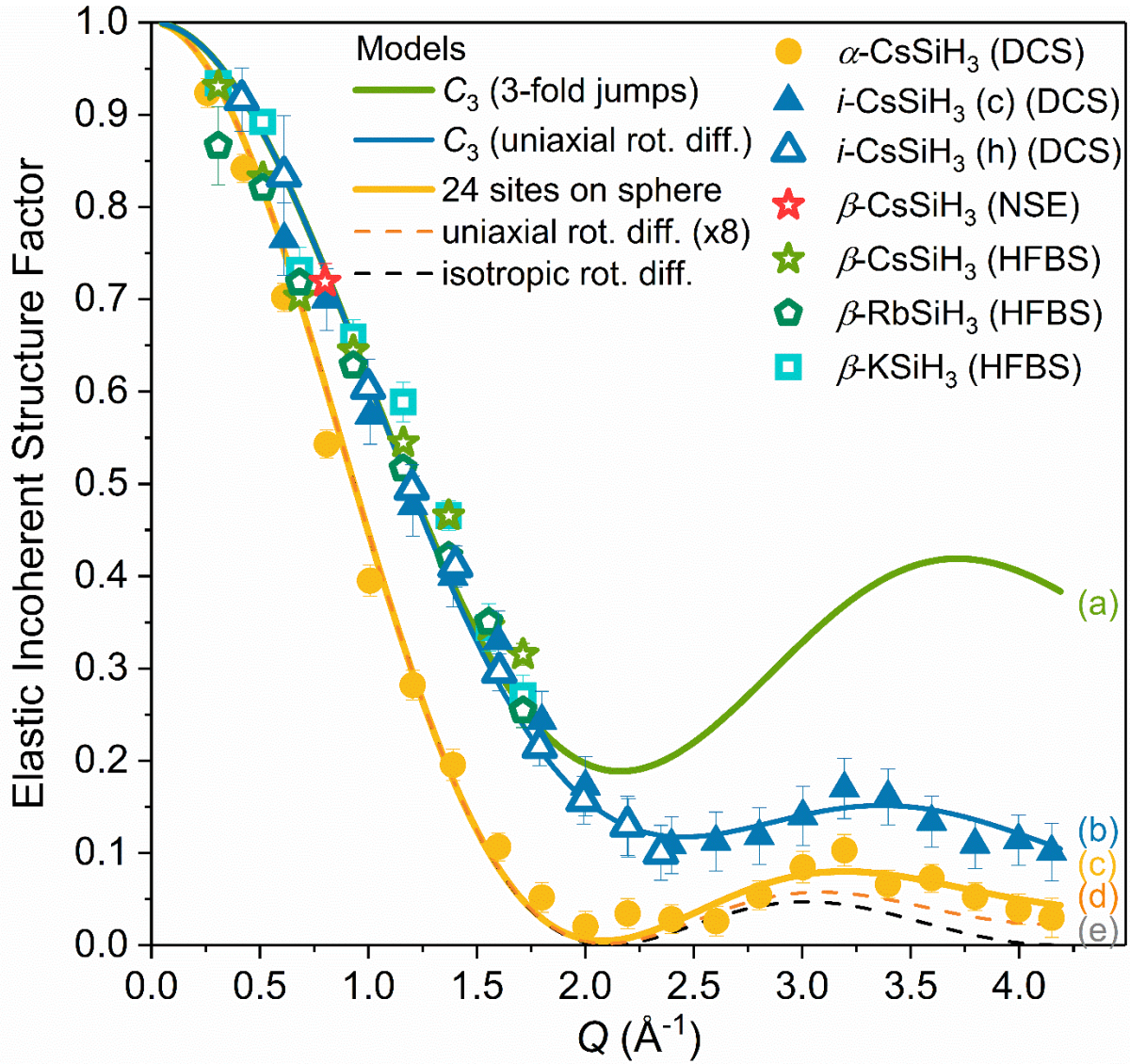


Figure 7. Elastic incoherent structure factor (EISF) data vs. Q for α -CsSiH₃ (orange circles, 270 K), i -CsSiH₃ (filled blue triangles (cooling)/open blue triangles (heating), 240 K), β -CsSiH₃ (open green and red stars, 200 K), β -RbSiH₃ (open dark green pentagons, 247 K), and β -KSiH₃ (open blue squares, 292 K). EISFs for α -CsSiH₃ and i -CsSiH₃ were derived from DCS measurements (2.75 Å and 4.8 Å neutrons), while those for β -KSiH₃, β -RbSiH₃, and β -CsSiH₃ from HFBS measurements. Open red star symbol denotes the EISF value for β -CsSiH₃ from NSE measurements at 140 K and $Q = 0.8 \text{ \AA}^{-1}$. EISF model curves for various anion reorientational mechanisms are shown for comparison: (a) three-fold jumps around the nominal anion C_3 symmetry axis, (b) rotational diffusion around the C_3 axis, (c) 24-site model involving three-fold jumps around eight differently aligned anion C_3 axes, (d) uniaxial rotational diffusion around eight differently aligned anion C_3 axes, and (e) isotropic rotational diffusion. (See the SI for further model details.)

The SiH_3^- anion reorientations for all β -phase compounds are crystallographically restricted by symmetry to follow a three-site jump model in which H atoms reorient by 120° jumps about the nominal three-fold SiH_3^- symmetry axis with an average H-H jump distance of $\approx 2.23 \text{ \AA}$.³ To have a reasonable agreement between the experimental data and this model, a fraction of immobile H atoms had to be included in all cases as extra elastic-peak intensity, e.g., (30 %) for $\beta\text{-KSiH}_3$ at 292 K, (10 %) for $\beta\text{-RbSiH}_3$ at 247 K, and (43 %) for $\beta\text{-CsSiH}_3$ at 200 K. Extra elastic-peak contributions are to be expected, most certainly reflecting “contamination” due to (i) the elastic-scattering fraction from much-more-highly-mobile SiH_3^- anions associated with coexisting i -phases and α -phases, and (ii) additional elastic-scattering contributions from immobile H atoms associated with other minor hydrogenous impurity phases. Coexisting MSiH_3 phases and other minor impurities such as MH are common in synthesized MSiH_3 compounds as borne out in this and previous studies.^{1,3,10,13} Although the high-resolution HFBS measurements will detect the associated elastic scattering from the extra i -phases and α -phases, the fraction of extremely broad quasielastic scattering that would normally be observable with the DCS spectrometer will remain largely outside the HFBS measurement window and invisible as part of the HFBS flat background. This uniaxial reorientational behavior is consistent with the additional higher-resolution NSE measurements performed on $\beta\text{-CsSiH}_3$ at the relatively low temperature of 140 K after heating from 4 K (see [Figure S2](#)), where the amounts of coexisting i -phase and α -phase and their concomitant excess elastic-peak contributions will be minimal.

We point out that, although it would be preferable to measure the β -phase EISFs out to higher Q values than shown in [Figure 7](#) to more clearly corroborate the rise in EISF values with increasing Q values above 2 \AA^{-1} as expected for a three-fold reorientational jump mechanism, we are limited by the HFBS spectrometer to Q values less than $\approx 1.7 \text{ \AA}^{-1}$. Nonetheless, the observed

Q -independent quasielastic linewidths in [Figure 3](#) for the β -phase compounds provide an independent confirmation for such a reorientational model.

In contrast to the uniaxial three-fold jump model describing the β -phase SiH_3^- reorientations, the α -phase SiH_3^- reorientations have been successfully described by a three-dimensional “24-site” model established previously,¹³ which utilizes the 24 positions of a corner-truncated cube as jump locations for H atoms, mimicking the various partially occupied H positions shown in [Figure 1](#). This model represents a composite mechanism comprised of both three-fold uniaxial reorientations of H atoms around the anion C_3 axis and the eight-fold flipping of this axis itself towards orientations that are aligned along the body diagonals of the cubic $Fm\bar{3}m$ unit cell. When considering this model, it is not unreasonable to assume that the anion actually uses its center of gravity as the (three-dimensional) reorientational pivot point, which is on the anion C_3 axis but offset towards the three H atoms by about 0.08 Å from the Si atom center (see [Figure S4](#)). If one further assumes that this pivot point (and not Si) is anchored at the high-symmetry Si position determined from refinement of the diffraction-averaged cubic α -phase structure,³ then the effective radius of the sphere surface visited by the three H atoms via a 24-site model is slightly smaller than the Si-H bond distance of ≈ 1.52 Å established from pair distribution functions for α -KSiD₃ and α -RbSiD₃ extracted from neutron total scattering data.¹¹ Rather, it is more in line with an “effective” Si-H bond distance of ≈ 1.47 Å to 1.49 Å determined by Rietveld refinement of α -MSiD₃ NPD data.³ Of course, this refined distance is measured from the average Si high-symmetry position at the center of the cube of eight surrounding alkali metal cations. In reality, the Si atom may actually be slightly off-center by ≈ 0.08 Å at any one of eight positions along the body diagonals. Indeed, the characteristically large NPD-derived atomic displacement parameters observed for Si in the α -phases compared to those for Si in the β -phases^{3,10} are

consistent with the existence of multiple off-center Si positions in the α -phases rather than perfectly centered Si atoms.

In line with the above discussion, we used the 24 H positions (extending radially 1.49 Å from the average Si high-symmetry position) for the α -CsSiH₃ 24-site-model analyses based on the NPD-derived α -CsSiH₃ structural model.³ As for α -KSiH₃ and α -RbSiH₃,¹³ this model, rather than one based on fully isotropic rotational diffusion, fits the α -CsSiH₃ data well in the temperature range from 350 K to 270 K (see [Figure S6](#)) after the experimental data are corrected for extra elastic scattering from an immobile fraction (14 %) of H atoms from minor hydrogenous impurity phases such as CsH as well as any trace amounts of lingering β -CsSiH₃ (and/or intermediate *i*-CsSiH₃) phase(s). A similar magnitude correction (10 %) was also previously necessary to attain better agreement with the 24-site model for α -KSiH₃ and α -RbSiH₃.¹³ Similar to our earlier justifications for the extra elastic scattering in the β -phase QENS data, the presence of lingering β -MSiH₃ and minor MH impurity phases in the α -MSiH₃ phases have also been observed by prior diffraction studies.^{1,3,10}

This 24-site model for α -CsSiH₃, which reflects three-fold reorientations of the H atoms around the eight possible crystal alignments of the SiH₃⁻ (C_3) axis of rotation, can be extended to consider more disordered uniaxial rotational diffusion around each differently aligned axis. Over the Q -range of these measurements, this can be well-approximated by merely considering six-fold (60°) jumps around each of the axes, instead of three-fold (120°) jumps, thus doubling the number of possible locations to consider. The details for determining the associated EISF can be found in the SI, and it is plotted in [Figure 7](#) and [Figure S6](#) for comparison with the experimental data. It is clear that there are only minor differences between the 24-site model and this more disordered model, which could be largely compensated for by very minor corrections (on the order of a per

cent) in the assumed immobile fraction of elastically scattered H present. Hence, although the 24-site model is simpler and seems sufficient to describe the anion reorientational behavior over our Q -range, we cannot rule out that we are actually observing an α -phase mechanism involving something closer to uniaxial rotational diffusion rather than three-fold reorientations around the eight differently aligned axes.

Finally, the EISF behavior of the narrower DCS Lorentzian component associated with the i -phase, which was additionally included in the fitting of the QENS data of α -CsSiH₃, is also exemplified in [Figure 7](#). This i -CsSiH₃ phase component is observed in the temperature region from around 280 K to 170 K, contributing the maximal (and overwhelming) fraction of the total quasielastic scattering intensity near 240 K (roughly 3-4 \times the intensity of the broader α -phase component) in both heating and cooling regimens. Hence, this was the temperature used to extract the i -CsSiH₃ EISF from the DCS data. Starting with the 240 K DCS data (in cooling), where 2.75 Å neutron wavelength measurements were available for a maximal Q -range, we already know the Q -dependent quasielastic intensities for the i -phase and α -phase. To derive the i -phase EISF, we need to isolate the i -phase elastic scattering contribution from the measured total elastic scattering intensity by removing, first, the amount of Q -dependent elastic scattering due to the minor α -phase fraction based on the amount of corresponding α -phase quasielastic scattering and assuming that the α -phase EISF followed the 24-site model, and second, the extra Q -independent elastic scattering from the known 14 % hydrogenous impurity fraction determined earlier during the analysis of the pure α -phase data at higher-temperatures. Without considering any further elastic scattering corrections from any trace fraction of coexisting β -phase (which can also be considered as an immobile phase within this DCS resolution window), the resulting i -phase EISF is shown in [Figure 7](#). Although, the data agree very well with the EISF curve corresponding to

the uniaxial three-fold jump model for Q values less than 2 \AA^{-1} , there are marked deviations in the higher- Q region. Yet, they do agree remarkably well with the EISF curve corresponding to the uniaxial rotational diffusion model (i.e., more diffuse SiH_3^- anion reorientations around the nominal C_3 symmetry axis) over all Q values. The agreement at low Q values for both uniaxial reorientation models and the good overall agreement with the uniaxial rotational diffusion model suggests that no further elastic scattering corrections are warranted. If any more elastic scattering corrections were to be made to account for additional trace β - CsSiH_3 , then the resulting i -phase EISF data points would approach closer to the EISF curve corresponding to the sphere-tracing 24-site model, but still deviate significantly with respect to the specific Q -dependent behavior expected, no matter how large of an additional correction is considered. Based on this observation, it is reasonable to assume that very little β - CsSiH_3 is indeed present.

A similar procedure was used to determine the i -phase EISF at 240 K (in heating), but only 4.8 \AA neutron wavelength DCS data were available, so the maximum Q value was only 2.35 \AA^{-1} . Nonetheless, the resulting data, also shown in [Figure 7](#), favor the same uniaxial rotational diffusion model as for the 240 K data in cooling.

The particular Q -dependent behavior (such as the functional shape and position of the first minimum) of the derived EISF for i - CsSiH_3 at 240 K (in both cooling and heating) points strongly to a uniaxial reorientational model around the anion C_3 axis as happens in the β -phase rather than a more-three-dimensional 24-site-type model as happens in the α -phase. Yet, it is important to note that the relatively more muted EISF oscillation at higher Q values further suggests that the i - CsSiH_3 anion reorientations around the C_3 symmetry axis are more delocalized than strictly 120° jumps, with the data following a uniaxial small-angular-jump rotational diffusion model reasonably well. The true uniaxial mechanism may be something in between three-fold jumps and

rotational diffusion, e.g., a partial angular delocalization of possible H positions at other orientations nearby the main three-fold positions. This type of delocalization model has been used to address the QENS measurements concerning the reorientations of BH_4^- anions in hexagonal phase of LiBH_4 .²¹ As the extent of this angular “smearing” of jump positions increases from no smearing to complete smearing (i.e., rotational diffusion), the characteristic EISF functional form with Q will gradually transform from the classic three-fold jump model to the rotational diffusion model. Although some N -dependent variation of the quasielastic linewidth with Q is expected for N -fold uniaxial jumps above $N=3$, a uniaxial rotational diffusion model (i.e., small-angular jumps for large N values) is not inconsistent with the muted Q -sensitivity of the quasielastic linewidth seen in Figure 6 over the measured Q -range, according to Bee’s analysis¹⁹ of the expected Q -dependence of the composite quasielastic scattering (fwhm) linewidth for the case of very small angular jumps ($N \geq 12$) around a circle. We note that such an intermediate uniaxial rotational diffusion model would be a particularly reasonable progression from a more ordered, uniaxial three-fold jump model in the β -phase to a less ordered, eight-axis version of uniaxial rotational diffusion (instead of the 24-site model) in the α -phase.

Nedumkandathil *et al.*¹⁰ have suggested from the EISF analysis of their QENS data for KSiH_3 and RbSiH_3 that the SiH_3^- anions in their remnant undercooled α -phases undergo uniaxial three-fold jumps around the C_3 axis. This is somewhat at odds with the more diffuse uniaxial reorientational mechanism deduced here for *i*- CsSiH_3 , although it is not clear at this point if we are interpreting dynamical phenomena from the same type of intermediate species as those identified as remnant undercooled α -phases in KSiH_3 and RbSiH_3 . Again, higher-resolution QENS measurements are ultimately needed across the transition regions for KSiH_3 and RbSiH_3 to better

understand the similarities and differences in dynamical behavior among the three MSiH_3 compounds.

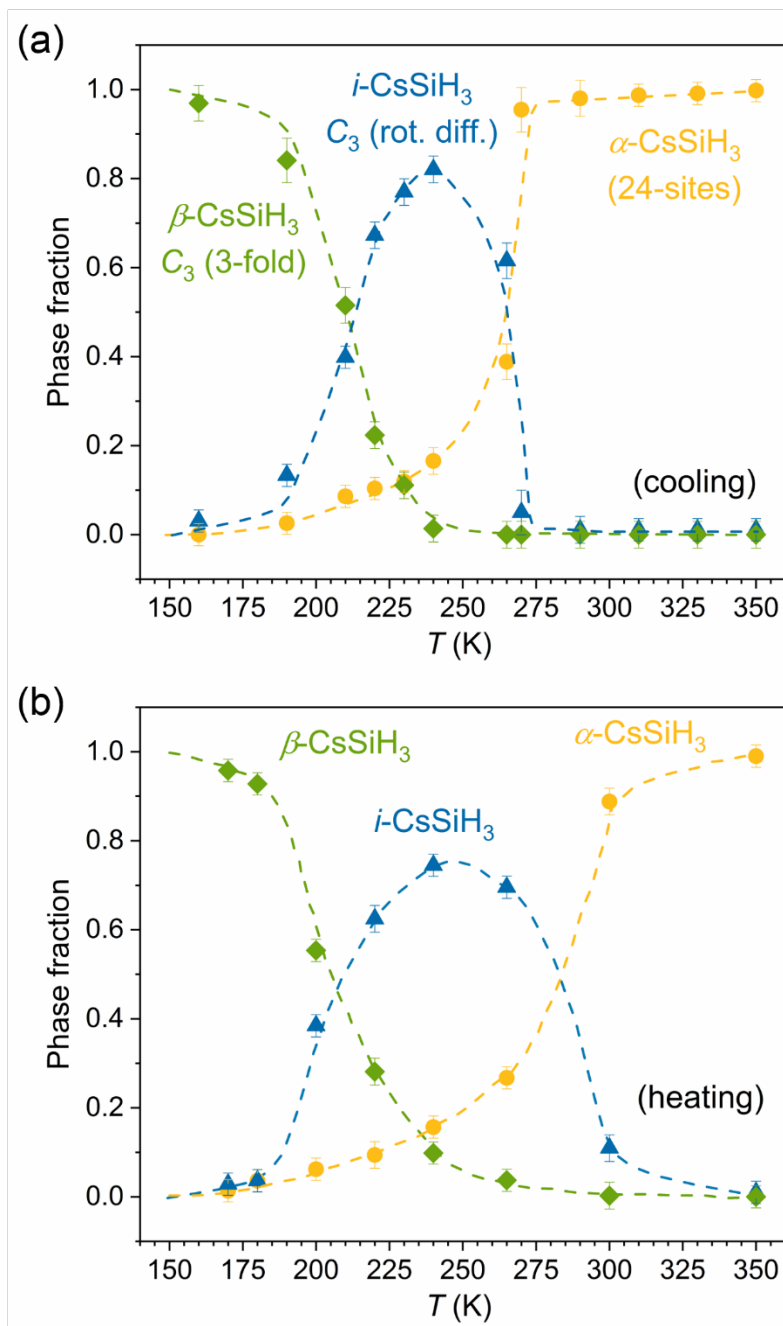


Figure 8. Phase diagrams for CsSiH_3 derived from anion dynamical behavior with temperature upon (a) cooling from 350 K and (b) heating from 25 K. The symbols present the calculation of the phase fractions obtained from QENS measurements, while the dashed lines represent guides to the eye.

It was informative to construct rough phase diagrams for CsSiH₃ (upon both cooling and heating regimens) based on integrated intensity analyses of the DCS QENS spectra with temperature at a single appropriate Q value (0.8 \AA^{-1} in this case). These are shown in [Figure 8](#). In particular, the phase fractions were estimated at a number of different measured temperatures under the assumption that the total integrated incoherent scattering intensity from all H atoms, which equals the summed intensities of all quasielastic and elastic components in the QENS spectra (without the extra intensity from the broad overdamped mode scattering component), is a constant (which is essentially ignoring the minor temperature-dependent effects of the Debye-Waller factor on intensity). Moreover, the molar fraction of each CsSiH₃ phase (α , i , and β) was assumed to be directly proportional to its total component scattering intensity. It was further assumed that the 24-site model and the uniaxial rotational diffusion model (and their associated EISFs) represent the respective anion reorientational behaviors for the α - and i -phases. The relative fraction of α - and i -phases at any given temperature can then be estimated by determining the total amount of scattering corresponding to each of these phases at $Q = 0.8 \text{ \AA}^{-1}$. The relative intensities of the quasielastic components for the α - and i -phases are obtained from the spectral component fits of the QENS spectrum at this Q value. The corresponding elastic intensities for each phase are then calculated from the respective EISF model values at this same Q value. Next, the total scattering intensity for each of the α - and i -phases is determined by summing the individual elastic and quasielastic component intensities. Finally, the relative fraction of the β -phase is determined from the residual elastic scattering intensity left over after subtracting the total scattering intensities due to the α -phase plus the i -phase plus the known impurity elastic scattering from the constant summed total scattering intensity (due to all phase fractions) as determined from the overall spectral component fits of the QENS spectrum mentioned above. This process is then repeated for

all measured temperatures. Based on this phase diagram for CsSiH₃, it is obvious that all three phases are indeed present over a broad intermediate temperature region, with a maximum *i*-phase fraction of about 75 % to 85 % present near 240 K. There appears to be a more pronounced transitional hysteresis occurring in the higher-temperature region between the α -phase and the *i*-phase than in the lower-temperature region between the β -phase and the *i*-phase, which helps to better understand the observed hysteresis due to changing mechanism and phase-fraction effects in the higher-temperature region of the FWS for CsSiH₃ in [Figure S1](#).

CsSiD₃ Temperature-dependent Structural Behavior

After establishing the QENS-derived CsSiH₃ phase diagrams in [Figure 8](#), it was highly informative to compare them to the temperature-dependent structural evolution of CsSiD₃ phases via NPD. [Figure 9](#) displays a subset of NPD patterns collected at progressively lower temperatures upon cooling from 299 K down to 162 K. (N.B., no NPD measurements were performed upon heating.) Ignoring any extremely subtle changes, e.g., such as a monoclinic to triclinic transformation analogous to that reported for β -RbSiD₃,¹⁰ there are no obvious signs of an additional long-range-ordered phase at the intermediate temperatures between the α - and β -phases, only a slight drop of roughly 15 % in the apparent mass of crystalline material in the transition region, as might typically be expected to accompany such a dramatic phase change. In particular, we took all of the NPD patterns collected and generated a rough phase diagram plot in [Figure 10](#) (analogous to those generated in [Figure 8](#)) by evaluating the areas under selected Bragg peaks as functions of temperature. The (200) reflection was chosen for the α -phase and the (301) + (202) reflections were chosen for the β -phase. The integrated peak intensities corresponding to each phase were normalized so that the values were unity at 299 K for the α -phase and at 162 K for the β -phase. Done in this way, the normalized peak intensities could also be considered as a measure

of the phase fractions of the crystalline portion of the CsSiD_3 . By summing the α - and β -phase fractions at each temperature, we could then deduce the extra fraction required to attain unity. This extra fraction approximates the loss of crystalline material during the phase transformation potentially due to a marked decrease in coherence lengths for a portion of this affected material and/or the nucleation of nanosized domains of a structurally distinct intermediate phase with local geometric arrangements that are different than (and intermediate to) those for the α - and β -phases.

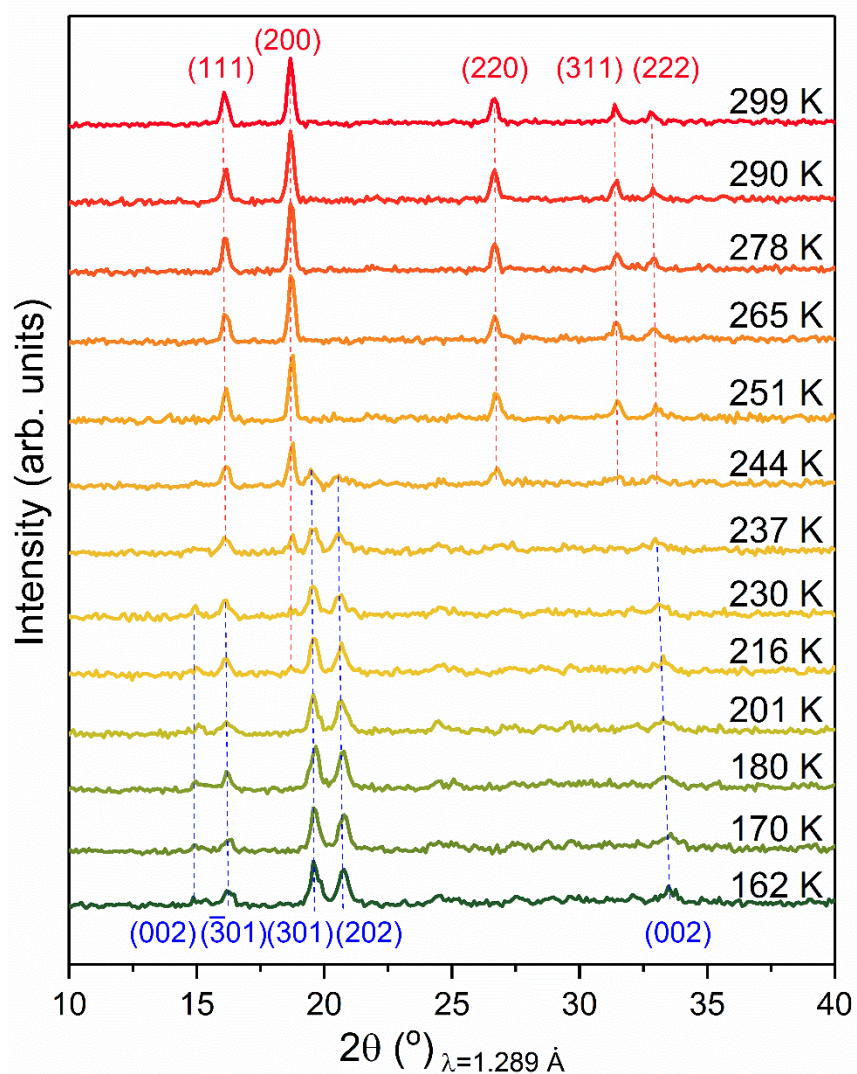


Figure 9. NPD patterns for CsSiD_3 upon cooling from 299 K to 162 K, indicating pertinent lattice reflections for the α -phase (top), which is the stable phase at the higher temperatures, and for the β -phase (bottom), which is the stable phase at the lower temperatures.

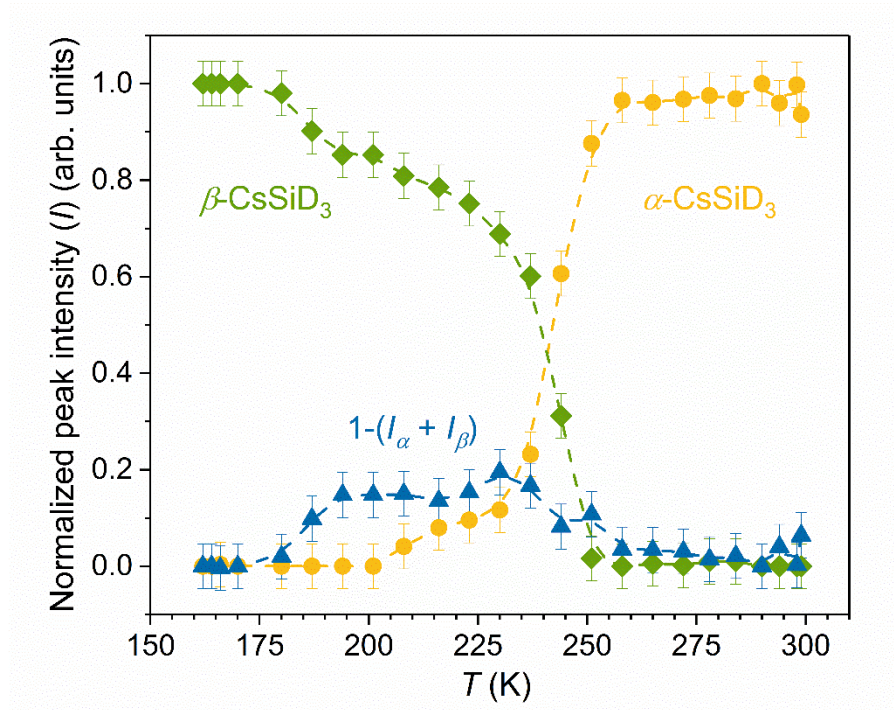


Figure 10. Evolution of the normalized NPD Bragg peak intensities for α -CsSiD₃ (yellow) and β -CsSiD₃ (green) with temperature upon cooling. Blue symbols represent the extra peak intensities at each temperature that must be added to the summed intensities for the α - and β -phases to attain unity.

Although we anticipate that CsSiD₃ will display minor temperature-related deviations in phase-transition behavior compared to CsSiH₃ with respect to the exact position and breadth of the transition region, it is reasonable to assume that CsSiD₃ and CsSiH₃ will be morphologically similar, allowing for a meaningful comparison of Figures 8 and 10. The missing fraction of crystalline CsSiD₃ material in Figure 10 is akin in thermal evolution to that of the *i*-phase fraction of CsSiH₃ material in Figure 8a, although the overwhelming magnitude (roughly 85 %) observed for the latter CsSiH₃ fraction at 240 K is over five-fold higher than that for the former CsSiD₃ fraction.

One must keep in mind that, although NPD senses only the coarser crystalline portion of the CsSiD₃, QENS is a highly local probe and detects all of the SiH₃⁻ anions in the CsSiH₃,

irrespective of crystallite size, so it provides a global tally of the anion dynamics. Even if these intermediate fractions in both figures happen to represent the same type of dynamically distinct, intermediate structural arrangements, the large discrepancy in phase fractions can only be reconciled if one assumes that (i) the CsSiH₃ is comprised predominantly of short-coherence-length nanodomains largely invisible to diffraction, with a minority of longer-coherence-length crystalline material, and (ii) the *i*-CsSiH₃ phase forms chiefly within these nanocrystalline domains, both upon cooling from the nano- α -phase and upon heating from the nano- β -phase, and remains stabilized over an extended intermediate temperature range. For the diffraction-visible, more coarsely crystalline material, [Figure 10](#) indicates a more abrupt transition from α -phase to β -phase, largely bypassing the stabilization of a similar intermediate structural arrangement extending down to lower temperatures as observed for the nanocrystalline fraction, before ultimately forming the β -phase. Depending on the exact nature (i.e., short-coherence-length α -, β -, or *i*-phase) of the 15 % amorphous-like material inferred by the CsSiD₃ NPD measurements in the intermediate temperature regime, the fraction of the shorter-range-ordered CsSiH₃ nanocrystallites present in the CsSiH₃ over the entire temperature range is estimated to be anywhere between 70 % to 85 %.

The existence of such a large fraction of amorphous-like nanomaterial is also fully consistent with the unusually large amount of diffuse scattering intensity, i.e., an order of magnitude more than the intensity under the NPD Bragg peaks, as highlighted for both α -CsSiD₃ and β -CsSiD₃ in [Figure S7](#). Moreover, instead of being fairly flat, the diffuse scattering background exhibits a rather dramatic broad hump that peaks in the Q region corresponding to what would be expected if the form factor were dominated by a single SiD₃⁻ anion. In reality, the diffuse background is rather smeared out since the nanodomains will have a distribution of short

coherence lengths, i.e., a broad distribution of different small unit-cell clusters to consider, although the hump is still an indication that the basic SiD_3^- geometric arrangement (and more specifically, the three D atoms) dominates the Q dependence. This diffuse scattering behavior can also be seen in past NPD patterns for KSiD_3 and RbSiD_3 ,³ which may signal that nanodomain formation is a general phenomenon occurring in these compounds during their synthesis. It would be interesting to see if one could somehow reduce the amount of nanomaterial in CsSiH_3 by, e.g., using different synthesis methods or prolonged higher-temperature annealing under H_2 pressure. Then it should be possible to mitigate the formation of the i -phase during temperature cycling.

Conclusions

QENS measurements were employed to gain deeper insights into the dynamical behavior of the SiH_3^- anions in the low-temperature ordered β -phases and the high-temperature disordered α -phases of the mono-alkali silanides (MSiH_3 , where $M = \text{K}, \text{Rb}, \text{and Cs}$), which have been recently proposed as possible materials for near-ambient hydrogen-storage systems. The results show that the β - α phase transition leads to dynamical changes corresponding to orders of magnitude more rapid reorientational motions of the pyramidal anions. Maximum jump frequencies of the β -phase anions near the β - α transitions vary from around 10^9 s^{-1} for β - KSiH_3 to 10^{10} s^{-1} and higher for β - RbSiH_3 and β - CsSiH_3 . Focusing on CsSiH_3 in and above this transition region, the expanded and disordered α - CsSiH_3 compound exhibits significantly higher anion reorientational jump frequencies approaching and exceeding 10^{12} s^{-1} , in accordance with prior QENS results. The lower anion mobilities in the ordered β -phases compared to the disordered α -phases are expected, due to the smaller (more sterically restrictive) unit cell volume for the former.

In contrast to the β -phases, which show significantly higher reorientation activation energies and larger deviations between different MSiH_3 compounds, relatively weaker temperature dependences of anion reorientational jump frequencies are observed for the α -phases with smaller differences in activation energies between the different congeners.

The single crystallographic orientations for each SiH_3^- anion in the ordered β -phases point to only one physically reasonable anion reorientational mechanism, i.e., uniaxial three-fold rotational jumps of the H atoms around the anion three-fold symmetry axis. The SiH_3^- reorientations in the disordered α - CsSiH_3 are adequately modeled by H jumps between 24 different jump locations distributed radially around the anion center of gravity, in line with the various H-site occupations determined from NPD, although we cannot rule out a more disordered model involving uniaxial rotational diffusion around the various possible crystal alignments of the anion C_3 symmetry axis. The unusual nature of the anion dynamical transformation upon transitioning between the α - and β -phases of CsSiH_3 was probed in more detail, corroborating the presence of a dynamically distinct intermediate phase (*i.e.*, our *i*-phase), which may possibly be related to the nanosized “undercooled α -phase” KSiH_3 and RbSiH_3 recently reported by Nedumkandathil *et al.* The comprehensive QENS results for CsSiH_3 suggest that the SiH_3^- anions associated with this *i*-phase possess an order-of-magnitude lower orientational mobility than that for α -phase anions (though an order-of-magnitude higher orientational mobility than that for β -phase anions), as well as a decreased reorientational dimensionality within the neutron resolution window to uniaxial small-angular jumps rather than something more akin to the three-dimensional α -phase anion motions. Although these dynamical and mechanistic details elucidated by QENS cannot by themselves provide any more definite insights concerning local structural symmetry of the *i*-phase, they suggest nonetheless that it possesses a unit cell volume per CsSiH_3 formula unit somewhere

between those for the α - and β -phases. In such an intermediate-sized unit cell, there is more anion space for more rapid uniaxial reorientations than in the β -phase, but not enough anion space to enable noticeably rapid three-dimensional eight-fold realignments of the anion C_3 axis as for the α -phase.

Finally, the combination of these QENS results for CsSiH₃ with complementary NPD results for CsSiD₃ strongly suggest that this structurally and dynamically distinct *i*-phase is chiefly associated with short-range-ordered nanodomains (invisible to diffraction), which dominate the CsSiH₃ sample. This is particularly interesting from a thermodynamics viewpoint, since it indicates that decreasing the coherence length towards the nano-regime enables the stabilization of a local structural arrangement over an extended temperature range for CsSiH₃ that is intermediate to the structural arrangements of the α - and β -phases. For more coarsely crystalline domains, the NPD results suggest a sharper transition region between α - and β -phases, although it is not yet clear if the apparent minor loss of crystallinity associated with these domains in the transition temperature region can be equated to the formation of any comparable *i*-phase-like nanodomains.

ASSOCIATED CONTENT

Supporting Information

Complementary QENS and NPD data; SiH_3^- schematic; details of EISF models. This material is available free of charge via the Internet at <http://pubs.acs.org>.

AUTHOR INFORMATION

Corresponding Author

*E-mail: mirjana.dimitrievska@nist.gov, mirjana.dimitrievska@nrel.gov

*Tel: +1 (301) 975-0403

Notes

The authors declare no competing financial interest.

ACKNOWLEDGMENTS

M. D. gratefully acknowledges research support from the Hydrogen Materials - Advanced Research Consortium (HyMARC), established as part of the Energy Materials Network under the U.S. Department of Energy, Office of Energy Efficiency and Renewable Energy (DOE EERE), Fuel Cell Technologies Office, under Contract No. DE-AC36-08GO28308. This work was performed, in part, within the assignment of the Russian Federal Agency of Scientific Organizations (program “Spin” No. AAAA-A18-118020290129-5). This work was supported, in part, by the DOE EERE under Grant No. DE-EE0002978, and utilized facilities supported in part by the National Science Foundation under Agreements DMR-0944772 and DMR-1508249. We would like to thank Drs. C. M. Brown, R. L. Cappelletti, and D. A. Neumann for useful discussions, and Dr. V. Nassif for her assistance with the NPD measurements.

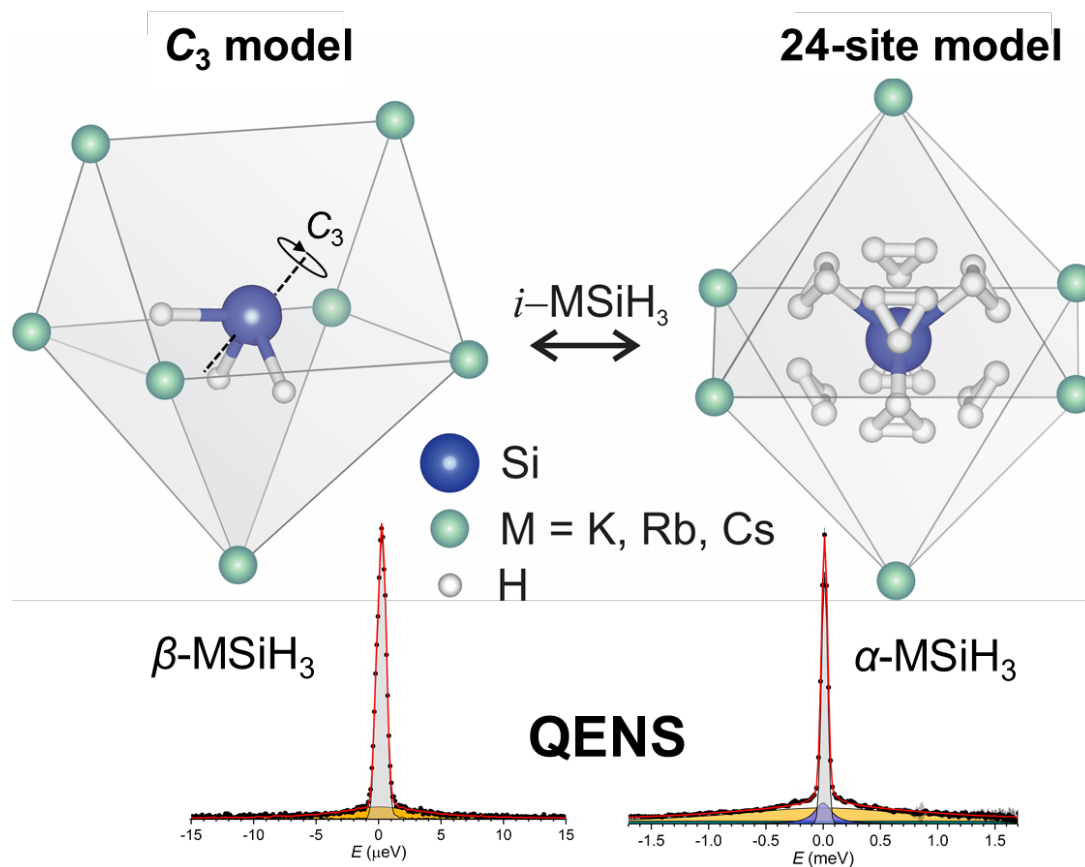
References

- (1) Chotard, J.-N.; Tang, W. S.; Raybaud, P.; Janot, R. Potassium Silanide (KSiH₃): A Reversible Hydrogen Storage Material. *Chem. – Eur. J.* **2011**, *17*, 12302–12309.
- (2) Tang, W. S.; Chotard, J.-N.; Raybaud, P.; Janot, R. Hydrogenation Properties of KSi and NaSi Zintl Phases. *Phys. Chem. Chem. Phys.* **2012**, *14*, 13319–13324.
- (3) Tang, W. S.; Chotard, J.-N.; Raybaud, P.; Janot, R. Enthalpy–Entropy Compensation Effect in Hydrogen Storage Materials: Striking Example of Alkali Silanides MSiH₃ (M = K, Rb, Cs). *J. Phys. Chem. C* **2014**, *118*, 3409–3419.
- (4) Jain, A.; Ichikawa, T.; Yamaguchi, S.; Miyaoka, H.; Kojima, Y. Catalytic Modification in Dehydrogenation Properties of KSiH₃. *Phys. Chem. Chem. Phys.* **2014**, *16*, 26163–26167.
- (5) Janot, R.; Tang, W. S.; Clémençon, D.; Chotard, J.-N. Catalyzed KSiH₃ as a Reversible Hydrogen Storage Material. *J. Mater. Chem. A* **2016**, *4*, 19045–19052.
- (6) Ring, M. A.; Ritter, D. M. Crystal Structure of Potassium Silyl. *J. Phys. Chem.* **1961**, *65*, 182–183.
- (7) Weiss, E.; Hencken, G.; Kühr, H. Kristallstrukturen und Kernmagnetische Breitlinienresonanz der Alkalisilyle SiH₃M (M = K, Rb, Cs). *Chem. Ber.* **1970**, *103*, 2868–2872.
- (8) Mundt, O.; Becker, G.; Hartmann, H.-M.; Schwarz, W. Metallderivate von Molekülverbindungen. II. Darstellung und Struktur des β-Kaliumsilanids. *Z. Für Anorg. Allg. Chem.* **1989**, *572*, 75–88

-
- (9) Tang, W. S.; Dimitrievska, M.; Chotard, J.-N.; Zhou, W.; Janot, R.; Skripov, A. V.; Udovic, T. J. Structural and Dynamical Trends in Alkali-Metal Silanides Characterized by Neutron-Scattering Methods. *J. Phys. Chem. C* **2016**, *120*, 21218–21227.
- (10) Nedumkandathil, R.; Jaworski, A.; Fischer, A.; Österberg, C.; Lin, Y.-C.; Karlsson, M.; Grins, J.; Pell, A. J.; Edén, M.; Häussermann, U. Investigation of the Order–Disorder Rotator Phase Transition in KSiH_3 and RbSiH_3 . *J. Phys. Chem. C* **2017**, *121*, 5241–5252.
- (11) Kranak, V. F.; Lin, Y.-C.; Karlsson, M.; Mink, J.; Norberg, S. T.; Häussermann, U. Structural and Vibrational Properties of Silyl (SiH_3^-) Anions in KSiH_3 and RbSiH_3 : New Insight into Si–H Interactions. *Inorg. Chem.* **2015**, *54*, 2300–2309.
- (12) Mink, J.; Lin, Y.-C.; Karlsson, M.; Österberg, C.; Udovic, T. J.; Fahlquist, H.; Häussermann, U. Vibrational properties of $\beta\text{-KSiH}_3$ and $\beta\text{-RbSiH}_3$: A Combined Raman and Inelastic Neutron Scattering Study. *J. Raman Spectrosc.* **2017**, *48*, 284–291.
- (13) Österberg, C.; Fahlquist, H.; Häussermann, U.; Brown, C. M.; Udovic, T. J.; Karlsson, M. Dynamics of Pyramidal SiH_3^- Ions in ASiH_3 ($A = \text{K}$ and Rb) Investigated with Quasielastic Neutron Scattering. *J. Phys. Chem. C* **2016**, *120*, 6369–6376.
- (14) The mention of all commercial suppliers in this paper is for clarity and does not imply the recommendation or endorsement of these suppliers by NIST.
- (15) Copley, J. R. D.; Cook, J. C. The Disk Chopper Spectrometer at NIST: A New Instrument for Quasielastic Neutron Scattering Studies. *Chem. Phys.* **2003**, *292*, 477–485.
- (16) Meyer, A.; Dimeo, R. M.; Gehring, P. M.; Neumann, D. A. The High-Flux Backscattering Spectrometer at the NIST Center for Neutron Research. *Rev. Sci. Instrum.* **2003**, *74*, 2759–2777.

-
- (17) Rosov, N.; Rathgeber, S.; Monkenbusch, M. Neutron Spin Echo Spectroscopy at the NIST Center for Neutron Research, in *Scattering from Polymers: Characterization by X-Rays, Neutrons, and Light*, P. Cebe, B. S. Hsaio, D. J. Lohse (Eds.), American Chemical Society Symposium Series Vol. 739, American Chemical Society, 1999, pp. 103–116.
- (18) Azuah, R. T.; Kneller, L. R.; Qiu, Y.; Tregenna-Piggott, P. L. W.; Brown, C. M.; Copley, J. R. D.; Dimeo, R. M. DAVE: A Comprehensive Software Suite for the Reduction, Visualization, and Analysis of Low Energy Neutron Spectroscopic Data. *J. Res. Natl. Inst. Stand. Technol.* **2009**, *114*, 341–358.
- (19) Bee, M. *Quasielastic Neutron Scattering, Principles and Applications in Solid State Chemistry, Biology and Materials Science*; Adam Hilger: Bristol, UK, **1988**.
- (20) Soloninin, A. V.; Dimitrievska, M.; Skoryunov, R. V.; Babanova, O. A.; Skripov, A. V.; Tang, W. S.; Stavila, V.; Orimo, S.; Udovic, T. J. Comparison of Anion Reorientational Dynamics in $\text{MCB}_9\text{H}_{10}$ and $\text{MB}_{10}\text{H}_{10}$ ($\text{M} = \text{Li}, \text{Na}$) via Nuclear Magnetic Resonance and Quasielastic Neutron Scattering Studies. *J. Phys. Chem. C* **2017**, *121*, 1000–1012.
- (21) Verdal, N.; Udovic, T. J.; Rush, J. J. The Nature of BH_4^- Reorientations in Hexagonal LiBH_4 . *J. Phys. Chem. C* **2012**, *116*, 1614–1618.

TOC



Supporting information for:

Tracking the Progression of Anion Reorientational Behavior between α -phase and β -phase Alkali-Metal Silanides MSiH_3 by Quasielastic Neutron Scattering

Mirjana Dimitrievska,^{†,‡,*} Jean-Noël Chotard,[§] Raphaël Janot,[§] Antonio Faraone,^{†,†} Wan Si Tang,^{†,†,Δ} Alexander V. Skripov,[#] and Terrence J. Udovic[†]

[†]NIST Center for Neutron Research, National Institute of Standards and Technology, Gaithersburg, MD 20899-6102, United States

[‡]National Renewable Energy Laboratory, Golden, CO 80401, United States

[§]Laboratoire de Réactivité et Chimie des Solides (LRCS), UMR 7314 CNRS, Université de Picardie Jules Verne, 33 rue Saint-Leu, 80039 Amiens Cedex, France

[†]Department of Materials Science and Engineering, University of Maryland, College Park, MD 20742-2115, United States

^ΔGeophysical Laboratory, Carnegie Institution of Washington, Washington, DC 20015, United States

[#]Institute of Metal Physics, Ural Branch of the Russian Academy of Sciences, Ekaterinburg 620990, Russia

*E-mail: mirjana.dimitrievska@nist.gov, mirjana.dimitrievska@nrel.gov

*Tel: +1 (301) 975-0403

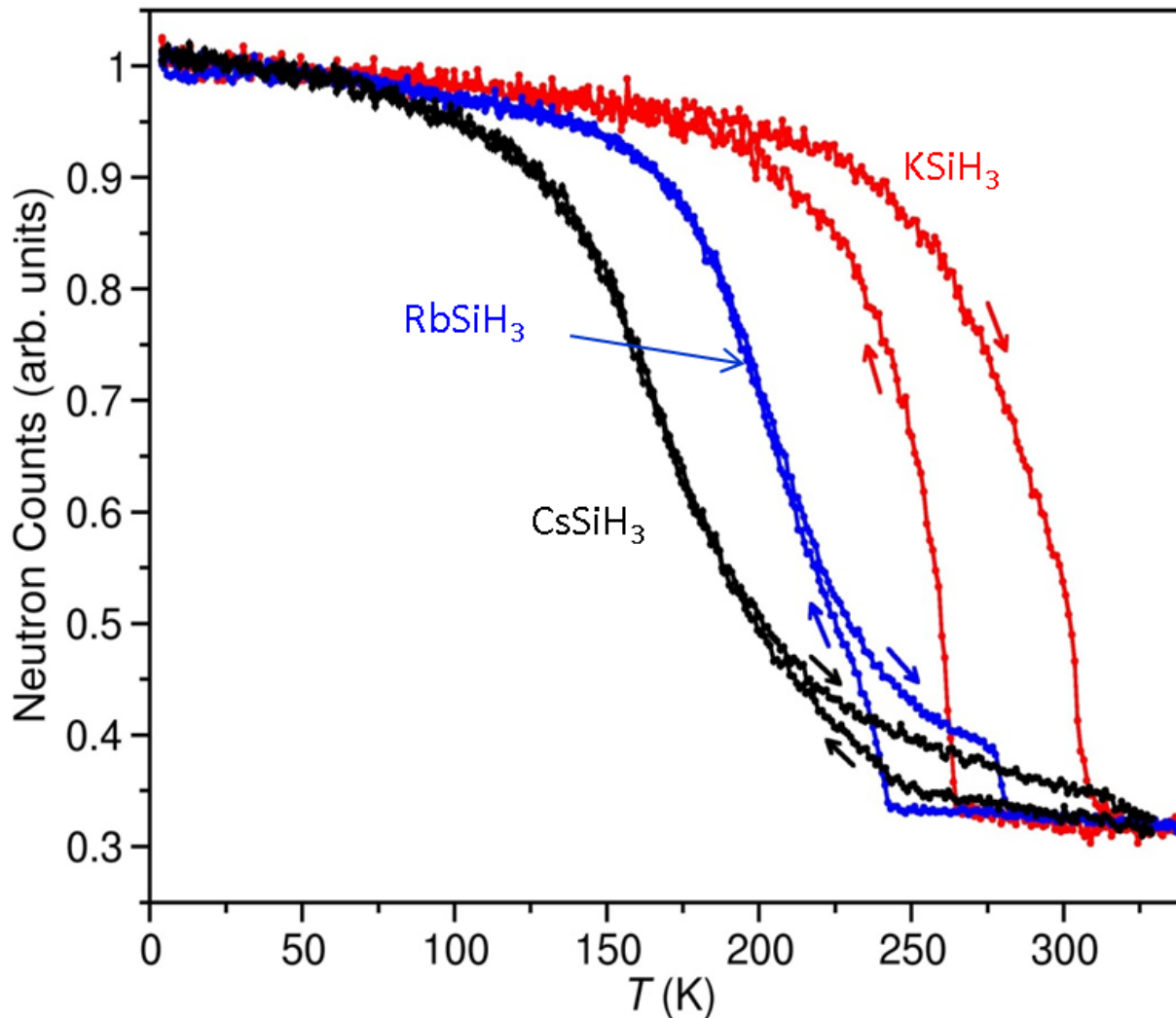


Figure S1. Neutron-elastic-scattering fixed-window scans (adapted from Ref. S1) using the HFBS spectrometer for the series of MSiH_3 compounds ($M = \text{K}, \text{Rb}, \text{and Cs}$) summed over detectors covering a Q range of 0.56 \AA^{-1} to 1.68 \AA^{-1} . Arrows differentiate scans during heating (from 4 K to 340 K) and cooling (from 340 K to 4 K). The final, more abrupt drop in intensities upon heating mark the β -phase to α -phase transition temperatures (ranging from $\sim 280 \text{ K}$, 305 K , and 320 K for $M = \text{K}, \text{Rb}$, and Cs , respectively). Hysteretic transformations back to elevated intensities can be seen upon cooling. The high-intensity plateaus at lower temperatures reflect SiH_3^- reorientational jump frequencies $< 10^8 \text{ s}^{-1}$ representative of β -phase anion mobilities, whereas the low-intensity plateaus at higher temperatures reflect much higher jump frequencies $\gg 10^{10} \text{ s}^{-1}$ representative of α -phase anion mobilities. Intermediate intensity regions reflect mobilities within the spectrometer resolution window (10^8 - $10^{10} \text{ jumps s}^{-1}$) and/or the summed effects from various fractional amounts of the different possible phases (α, i, β) present at a given temperature. Standard uncertainties are commensurate with the scatter in the data.

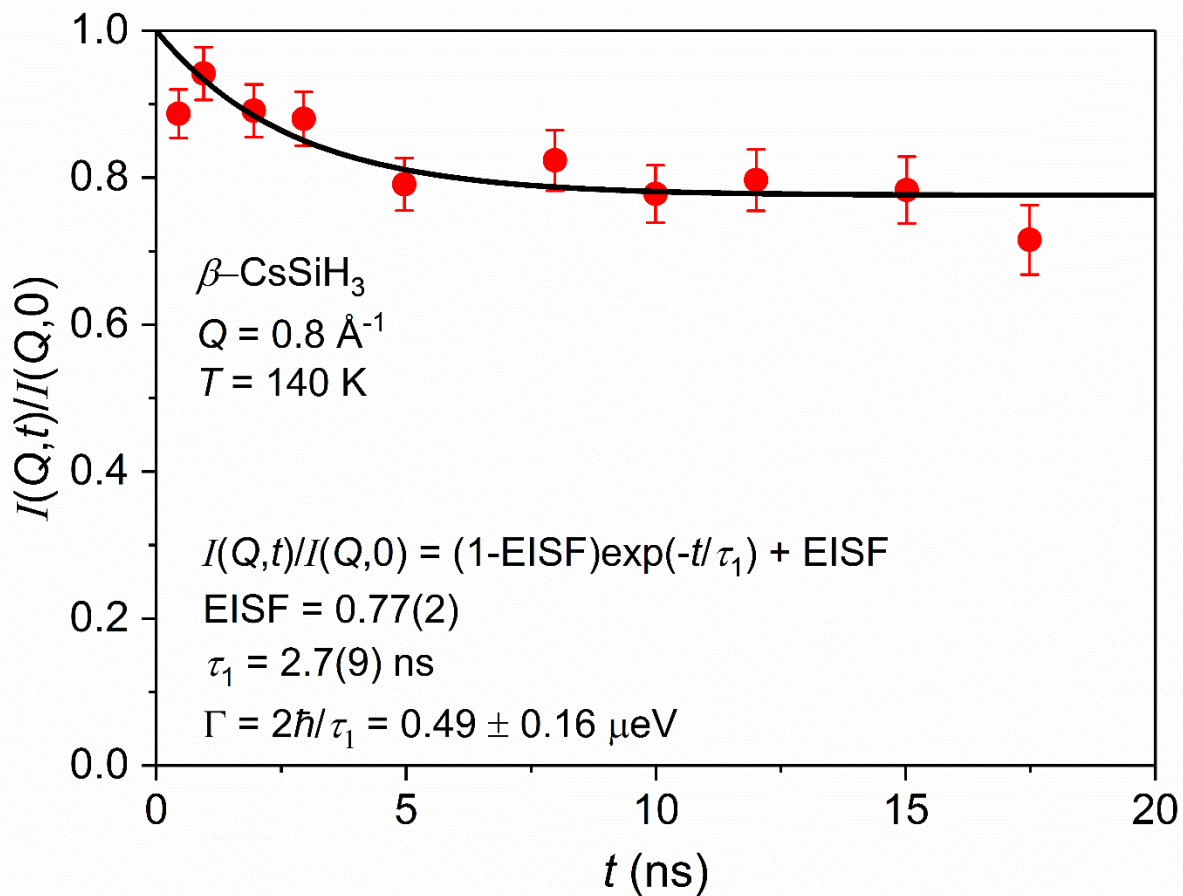


Figure S2. NSE measurements of β -CsSiH₃ at 140 K (after heating from 4 K) and $Q=0.8 \text{ \AA}^{-1}$ using 6.0 \AA neutrons. The model fit of the normalized intermediate scattering function $I(Q,t)/I(Q,0)$ yields an EISF of $0.77(2)$ and a τ_1 of $2.7(9) \text{ ns}$, which translates into a quasielastic fwhm linewidth Γ of $0.49 \pm 0.16 \text{ } \mu\text{eV}$. N.B., in neutron-spin-echo measurements, the intermediate scattering function $I(Q,t)$ is directly measured using the precession of the neutron spin in a magnetic field. The intensity decay is related to the anion reorientational dynamics. Vertical error bars denote $\pm 1\sigma$.

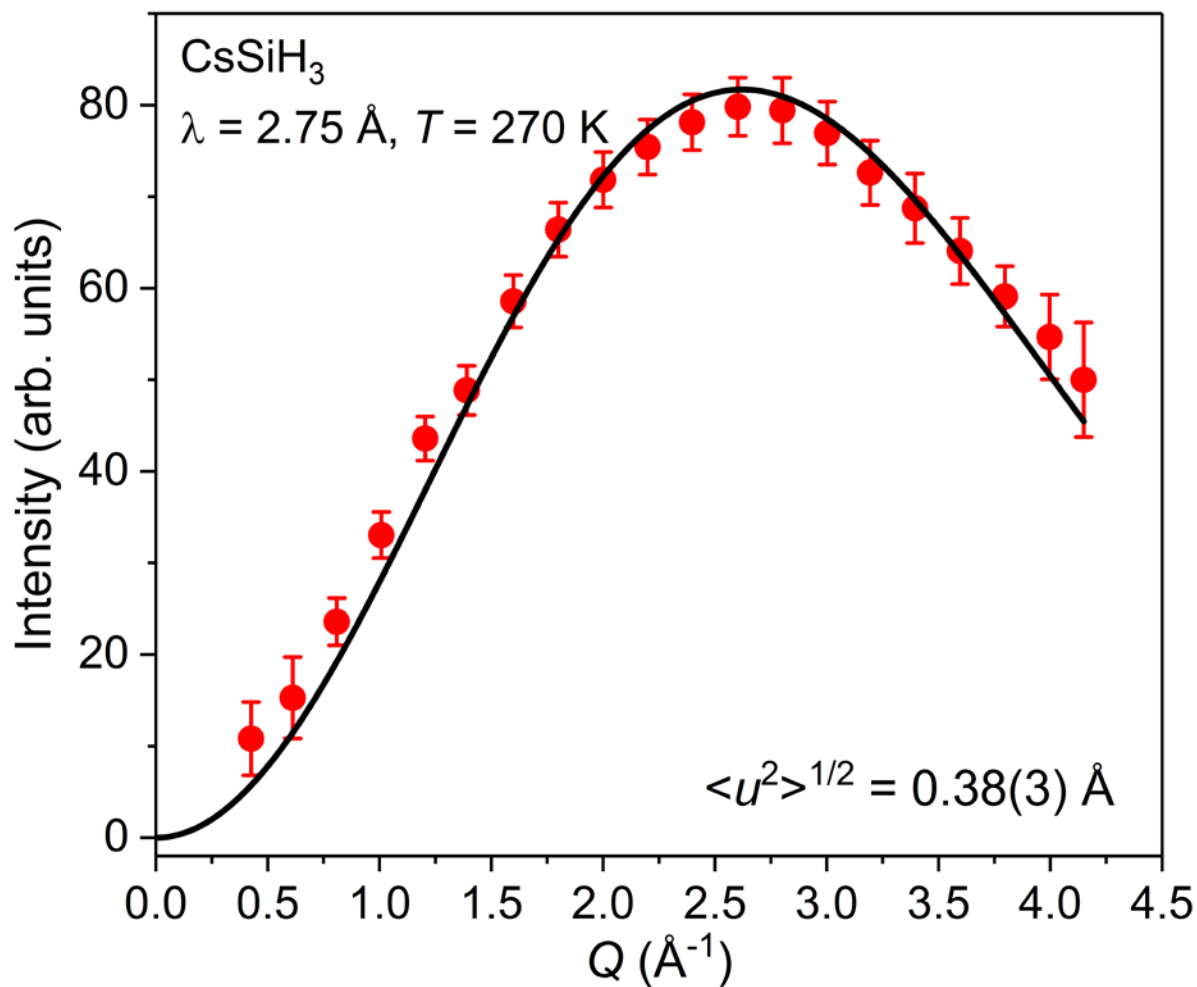


Figure S3. Q -dependence of the broader “overdamped-vibration” component intensity for CsSiH₃. The data were fit according to the incoherent neutron scattering law for a harmonic oscillator in the case of the one-phonon approximation: $I = A Q^2 \exp(-\langle u^2 \rangle Q^2)$, where I is the scattering intensity of the broader component, A is a constant, and $\exp(-\langle u^2 \rangle Q^2)$ is the Debye-Waller factor, with $\langle u^2 \rangle$ being the mean-squared displacement of the H atoms. The derived root-mean-squared displacement ($\langle u^2 \rangle^{1/2}$) is 0.38(3) Å. Vertical error bars denote $\pm 1\sigma$.

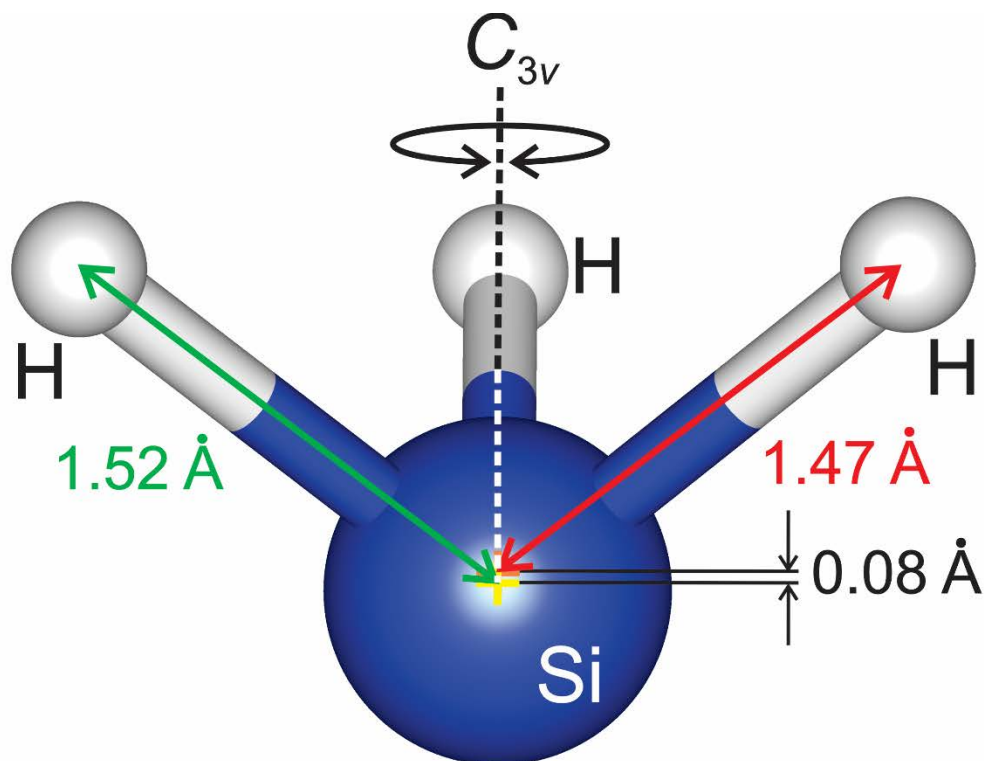


Figure S4. Schematic of the pyramidal SiH_3^- anion in $\alpha\text{-MSiH}_3$ oriented so that the C_{3v} local symmetry axis is vertical and in the plane of the page. A yellow cross denotes the geometric center of the Si atom. The Si-H and H-H bond distances are ~ 1.52 Å and ~ 2.19 Å, respectively, with H-Si-H bond angles of $\sim 92.2^\circ$, based on the pair distribution function results of neutron total scattering data.^{S2} An orange cross denotes the SiH_3^- center of gravity, which lies on the C_{3v} axis ~ 0.08 Å above the geometric Si center. The three-dimensional SiH_3^- reorientations prevalent in the α -phases likely use a pivot point closer to the center of gravity instead of the geometric Si center, which leads to a slightly reduced spherical radius of travel for the H atoms of ~ 1.47 Å and a counterbalancing (wobbling) Si atom tracing out a much smaller 0.08 Å spherical radius of travel. Compared to $\alpha\text{-MSiH}_3$, the SiH_3^- anion in $\beta\text{-MSiH}_3$ has a somewhat reduced symmetry with two slightly different values each for the Si-H and H-H bond distances and the Si-H-Si bond angles. The average respective distances and angle for M= K, Rb, and Cs are ~ 1.54 Å, 2.23 Å, and 92.8° .^{S3} all slightly larger values than for the α -phase. SiH_3^- reorientations in $\beta\text{-MSiH}_3$ are crystallographically restricted to undergoing three-fold jumps around the nominal anion C_3 axis.

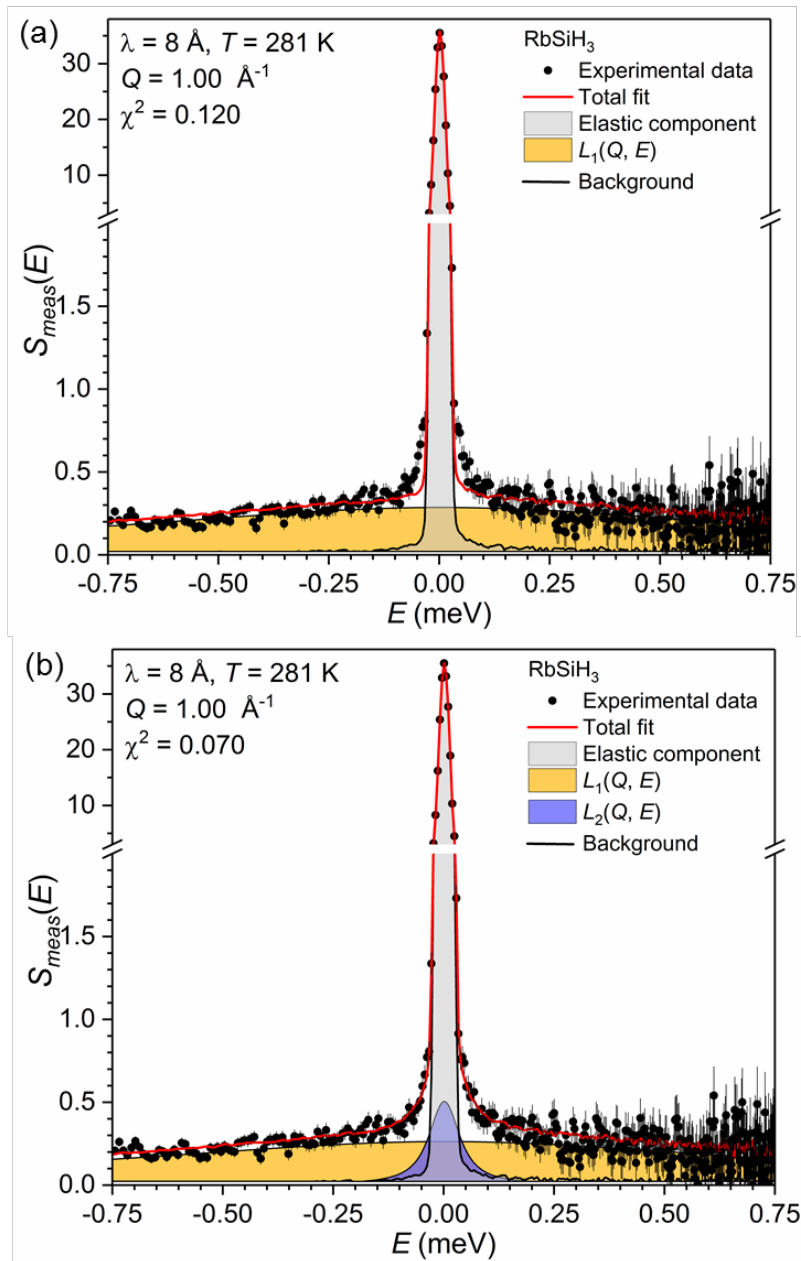


Figure S5. Exemplary QENS spectra for RbSiH₃ at 281 K and $Q = 1.00 \text{ \AA}^{-1}$ measured using 8 \AA wavelength neutrons (with 30 μeV fwhm resolution). Spectra were fit with a delta function and either (a) one or (b) two Lorentzian components, all convoluted with the instrumental resolution function, on top of a flat background. Figure (a) clearly indicates the need for including another narrower Lorentzian component attributed to a roughly 10 % fraction of significantly less reorientationally mobile SiH₃⁻ anions, as shown in Figure (b). N.B., it was not necessary to include a third overly broad Lorentzian component due to the overdamped vibrational contributions in these fits, since it blends into the flat background at this particular resolution, range, and Q value. Vertical error bars denote $\pm 1\sigma$.

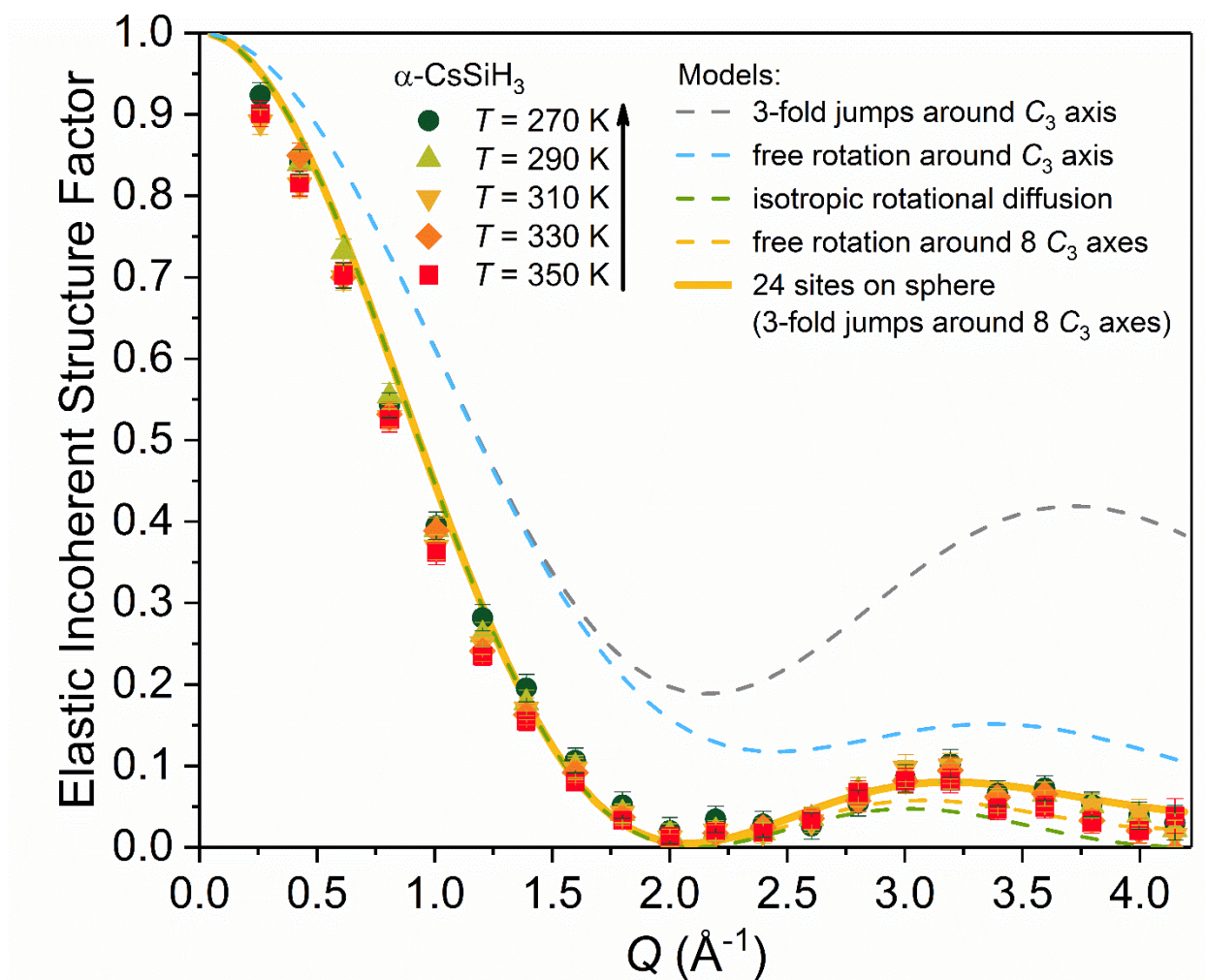


Figure S6. Temperature dependence of the elastic incoherent structure factor (EISF) data vs. Q for CsSiH_3 derived from QENS measurements with 2.75 \AA neutrons. EISF model curves for various anion reorientational mechanisms are shown for comparison. In all cases, the experimental data is corrected for an extra immobile fraction (14 %) of H atoms as discussed in the text. Vertical error bars denote $\pm 1\sigma$.

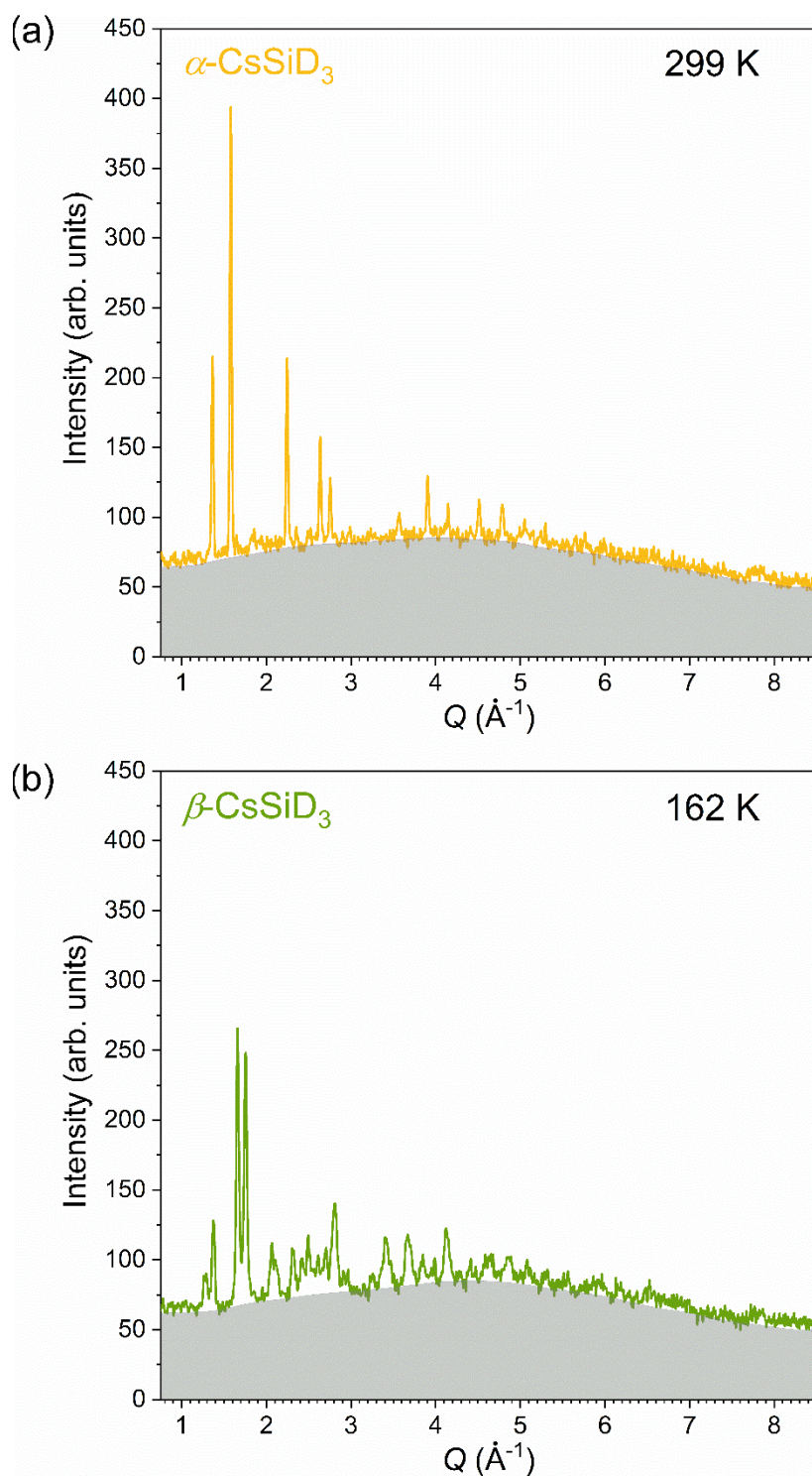


Figure S7. NPD patterns for (a) α -CsSiD₃ (at 299 K) and (b) β -CsSiD₃ (at 162 K) showing the order-of-magnitude larger amount of diffuse scattering background (highlighted in gray) compared to the amount of Bragg scattering. The broad hump is generally consistent with the form factor effects of the SiD₃⁻ anion present and the complex distribution of possible nanocluster arrangements. Standard uncertainties are commensurate with the scatter in the data.

Elastic Incoherent Structure Factor Models Corresponding to QENS Measurements

For the reorientational dynamics of an SiH_3^- “rigid-body” anion situated within a solid lattice such as MSiH_3 ($M = \text{K, Rb, or Cs}$), the EISF due to the H atoms reorienting around the central Si atom is sensitive to the fundamental details of the reorientational mechanism.

The mathematical expressions for the possible EISF models are shown below. Their derivation can be found elsewhere.^{S4-S7}

The EISF for a uniaxial three-fold jump model, where the reorientation of the three hydrogen atoms occurs about the nominal anion C_3 symmetry axis intersecting the stationary Si atom, is defined as:

$$\text{EISF}_{C_3} = \frac{1}{3} (1 + 2 j_0(Q d_{H-H}))$$

where $j_0(x)$ is a zeroth-order Bessel function equal to $\sin(x)/x$, and d_{H-H} is the jump distance between two SiH_3^- hydrogen atoms. The average β -phase and α -phase values are 2.23 Å and 2.19 Å.^{S2,S3}

The EISF for a uniaxial rotational diffusion model around the C_3 axis is defined as:

$$\text{EISF}_{C_3 \text{ rot.}} = \frac{1}{N} \sum_{i=1}^N j_0 \left(2 Q r \sin \left(\frac{\pi}{N} i \right) \right)$$

where N is large (≥ 50) and the rotational diffusion may be considered as free diffusion around a circle with radius $r = \frac{1}{\sqrt{3}} d_{H-H}$. N.B, for $N=3$, this model is identical to the uniaxial three-fold

jump model above. Already for $N \geq 6$ (small discrete jumps), the resulting EISF is hardly distinguishable from that for uniaxial rotational diffusion over the Q -range sampled in this study.

The EISF for a three-dimensional jump diffusion model on a sphere with 24 different jump locations is defined as:

$$\text{EISF}_{24\text{-site}} = \text{EISF}_{C_3 \times 8} = \frac{1}{24} (1 + 2 j_0(Q d_1) + j_0(Q d_2) + 4 j_0(Q d_3) + 2 j_0(Q d_4) + 2 j_0(Q d_5) + 2 j_0(Q d_6) + 2 j_0(Q d_7) + 4 j_0(Q d_8) + j_0(Q d_9) + 2 j_0(Q d_{10}) + j_0(Q d_{11}))$$

where d_i ($i = 1$ to 11) correspond to the 11 different H jump distances among the 24 locations in α -MSiH₃ as determined on the basis of neutron diffraction data.^{S3} These distances are given in [Table S1](#). This model corresponds to three-fold (120°) anion reorientations around each of eight different crystal alignments of the anion C_3 symmetry axis along the body diagonals of the cubic $Fm\text{-}3m$ unit cell. It has been found to adequately describe SiH₃⁻ reorientations within α -MSiH₃.^{S1,S7}

The EISF for a modified three-dimensional jump diffusion model on a sphere that now allows for uniaxial rotational diffusion around each of the eight differently aligned C_3 axes can be adequately approximated in our Q -range by a doubling of the possible H positions around each axis to six instead of three. In this approximation, each H atom now performs six-fold (60°) jumps around each axis, thus doubling the number of site locations to 48 (although the 24 additional locations reduce to only six with four-fold redundancies). This yields an EISF based on the equal contributions from two crystallographic types of H atoms, i.e., the original 24 H atoms and now the additional 24 H atoms. This results in an EISF based on two sets of terms corresponding to the different possible H jump distances (see [Table S1](#)) involving each respective type of H atom:

$$\text{EISF}_{C_3 \text{ rot.}} \times 8 =$$

$$\begin{aligned} & \frac{1}{2} \cdot \frac{1}{48} (1 + 2 j_0(Q d_1) + j_0(Q d_2) + 4 j_0(Q d_3) + 2 j_0(Q d_4) + 2 j_0(Q d_5) + 2 j_0(Q d_6) + \\ & 2 j_0(Q d_7) + 4 j_0(Q d_8) + j_0(Q d_9) + 2 j_0(Q d_{10}) + j_0(Q d_{11}) + 8 j_0(Q d_{12}) + 4 j_0(Q d_{13}) + \\ & 4 j_0(Q d_{14}) + 8 j_0(Q d_{15})) + \frac{1}{2} \cdot \frac{1}{48} (4 + 4 j_0(Q d_{11}) + 8 j_0(Q d_{12}) + 4 j_0(Q d_{13}) + \\ & 4 j_0(Q d_{14}) + 8 j_0(Q d_{15}) + 16 j_0(Q d_{16})) = \\ & \frac{1}{96} (5 + 2 j_0(Q d_1) + j_0(Q d_2) + 4 j_0(Q d_3) + 2 j_0(Q d_4) + 2 j_0(Q d_5) + 2 j_0(Q d_6) + \\ & 2 j_0(Q d_7) + 4 j_0(Q d_8) + j_0(Q d_9) + 2 j_0(Q d_{10}) + 5 j_0(Q d_{11}) + 16 j_0(Q d_{12}) + \\ & 8 j_0(Q d_{13}) + 8 j_0(Q d_{14}) + 16 j_0(Q d_{15}) + 16 j_0(Q d_{16})) . \end{aligned}$$

Table S1. Various H-H jump distances for SiH_3^- reorientational mechanisms in $\alpha\text{-CsSiH}_3$

i	H-H jump distances d_i (Å)	
1	0.728	Possible jump distances between 24 H locations
2	0.965	
3	1.566	
4	1.994	
5	2.092	
6	2.123	
7	2.215	
8	2.536	
9	2.820	
10	2.890	
11	2.980	
12	1.212	Additional jump distances due to 24 more H locations
13	1.733	
14	2.425	
15	2.723	
16	2.107	

Finally, the EISF for an isotropic rotational diffusion model on a sphere is defined as:

$$\text{EISF}_{iso} = j_0^2(Q r_{iso}).$$

In this case, the pyramidal SiH_3^- anion may be seen to rotate freely in all directions with jump distances corresponding to the surface of a sphere with radius r_{iso} . If one assumes that the Si atom is at the center of the sphere, then $r_{iso} = d_{\text{Si-H}}$. In reality, the SiH_3^- center of gravity is likely at the center of the sphere. In this case r_{iso} is slightly less than $d_{\text{Si-H}}$. See [Figure S4](#) for details.

References

- S1 Tang, W. S.; Dimitrievska, M.; Chotard, J.-N.; Zhou, W.; Janot, R.; Skripov, A. V.; Udovic, T. J. Structural and Dynamical Trends in Alkali-Metal Silanides Characterized by Neutron-Scattering Methods. *J. Phys. Chem. C* **2016**, *120*, 21218–21227.
- S2 Kranak, V. F.; Lin, Y.-C.; Karlsson, M.; Mink, J.; Norberg, S. T.; Häussermann, U. Structural and Vibrational Properties of Silyl (SiH_3^-) Anions in KSiH_3 and RbSiH_3 : New Insight into Si–H Interactions. *Inorg. Chem.* **2015**, *54*, 2300–2309.
- S3 Tang, W. S.; Chotard, J.-N.; Raybaud, P.; Janot, R. Enthalpy–Entropy Compensation Effect in Hydrogen Storage Materials: Striking Example of Alkali Silanides MSiH_3 ($M = \text{K}, \text{Rb}, \text{Cs}$). *J. Phys. Chem. C* **2014**, *118*, 3409–3419.
- S4 Bee, M. *Quasielastic Neutron Scattering, Principles and Applications in Solid State Chemistry, Biology and Materials Science*: Adam Hilger: Bristol, UK, **1988**.
- S5 Yildirim, T.; Gehring, P. M.; Neumann, D. A.; Eaton, P. E.; and Emrick, T. Neutron-Scattering Investigation of Molecular Reorientations in Solid Cubane. *Phys. Rev. B* **1999**, *60*, 314–321.
- S6 Dianoux, A. J.; Volino F.; Hervet, H. Incoherent Scattering Law for Neutron Quasi-Elastic Scattering in Liquid Crystals. *Mol. Phys.* **1975**, *30*, 1181–1194.
- S7 Österberg, C.; Fahlquist, H.; Häussermann, U.; Brown, C. M.; Udovic, T. J.; Karlsson, M. Dynamics of Pyramidal SiH_3^- Ions in ASiH_3 ($A = \text{K}$ and Rb) Investigated with Quasielastic Neutron Scattering. *J. Phys. Chem. C* **2016**, *120*, 6369–6376.